

**NONCLASSICAL PROPERTIES OF PULSED
SECOND-SUBHARMONIC GENERATION
IN PHOTONIC-BAND-GAP STRUCTURES**

**Final Technical Report
by**

**Dr. Jan Peřina
Dr. Ondřej Haderka
Dr. Michael Scalora
(April 2007)**

United States Army

EUROPEAN RESEARCH OFFICE OF THE U.S. ARMY

London, England

CONTRACT NUMBER: N62558-05-P-0421

Contractor: Univerzita Palackeho v Olomouci, Faculty of Natural Sciences, Dr. Jan Peřina, Joint Laboratory of Optics, 17. listopadu 50a, Olomouc, Czech Republic, 772 07

Approved for Public Release; distribution unlimited

REPORT DOCUMENTATION PAGE					<i>Form Approved OMB No. 0704-0188</i>	
<small>The public reporting burden for this collection of information is estimated to average 1 hour per response, including the time for reviewing instructions, searching existing data sources, gathering and maintaining the data needed, and completing and reviewing the collection of information. Send comments regarding this burden estimate or any other aspect of this collection of information, including suggestions for reducing the burden, to Department of Defense, Washington Headquarters Services, Directorate for Information Operations and Reports (0704-0188), 1215 Jefferson Davis Highway, Suite 1204, Arlington, VA 22202-4302. Respondents should be aware that notwithstanding any other provision of law, no person shall be subject to any penalty for failing to comply with a collection of information if it does not display a currently valid OMB control number.</small>						
PLEASE DO NOT RETURN YOUR FORM TO THE ABOVE ADDRESS.						
1. REPORT DATE (DD-MM-YYYY)		2. REPORT TYPE			3. DATES COVERED (From - To)	
4. TITLE AND SUBTITLE				5a. CONTRACT NUMBER		
				5b. GRANT NUMBER		
				5c. PROGRAM ELEMENT NUMBER		
6. AUTHOR(S)				5d. PROJECT NUMBER		
				5e. TASK NUMBER		
				5f. WORK UNIT NUMBER		
7. PERFORMING ORGANIZATION NAME(S) AND ADDRESS(ES)					8. PERFORMING ORGANIZATION REPORT NUMBER	
9. SPONSORING/MONITORING AGENCY NAME(S) AND ADDRESS(ES)					10. SPONSOR/MONITOR'S ACRONYM(S)	
					11. SPONSOR/MONITOR'S REPORT NUMBER(S)	
12. DISTRIBUTION/AVAILABILITY STATEMENT						
13. SUPPLEMENTARY NOTES						
14. ABSTRACT						
15. SUBJECT TERMS						
16. SECURITY CLASSIFICATION OF:			17. LIMITATION OF ABSTRACT	18. NUMBER OF PAGES	19a. NAME OF RESPONSIBLE PERSON	
a. REPORT	b. ABSTRACT	c. THIS PAGE			19b. TELEPHONE NUMBER (Include area code)	

INSTRUCTIONS FOR COMPLETING SF 298

1. REPORT DATE. Full publication date, including day, month, if available. Must cite at least the year and be Year 2000 compliant, e.g. 30-06-1998; xx-06-1998; xx-xx-1998.

2. REPORT TYPE. State the type of report, such as final, technical, interim, memorandum, master's thesis, progress, quarterly, research, special, group study, etc.

3. DATES COVERED. Indicate the time during which the work was performed and the report was written, e.g., Jun 1997 - Jun 1998; 1-10 Jun 1996; May - Nov 1998; Nov 1998.

4. TITLE. Enter title and subtitle with volume number and part number, if applicable. On classified documents, enter the title classification in parentheses.

5a. CONTRACT NUMBER. Enter all contract numbers as they appear in the report, e.g. F33615-86-C-5169.

5b. GRANT NUMBER. Enter all grant numbers as they appear in the report, e.g. AFOSR-82-1234.

5c. PROGRAM ELEMENT NUMBER. Enter all program element numbers as they appear in the report, e.g. 61101A.

5d. PROJECT NUMBER. Enter all project numbers as they appear in the report, e.g. 1F665702D1257; ILIR.

5e. TASK NUMBER. Enter all task numbers as they appear in the report, e.g. 05; RF0330201; T4112.

5f. WORK UNIT NUMBER. Enter all work unit numbers as they appear in the report, e.g. 001; AFAPL30480105.

6. AUTHOR(S). Enter name(s) of person(s) responsible for writing the report, performing the research, or credited with the content of the report. The form of entry is the last name, first name, middle initial, and additional qualifiers separated by commas, e.g. Smith, Richard, J, Jr.

7. PERFORMING ORGANIZATION NAME(S) AND ADDRESS(ES). Self-explanatory.

8. PERFORMING ORGANIZATION REPORT NUMBER. Enter all unique alphanumeric report numbers assigned by the performing organization, e.g. BRL-1234; AFWL-TR-85-4017-Vol-21-PT-2.

9. SPONSORING/MONITORING AGENCY NAME(S) AND ADDRESS(ES). Enter the name and address of the organization(s) financially responsible for and monitoring the work.

10. SPONSOR/MONITOR'S ACRONYM(S). Enter, if available, e.g. BRL, ARDEC, NADC.

11. SPONSOR/MONITOR'S REPORT NUMBER(S). Enter report number as assigned by the sponsoring/monitoring agency, if available, e.g. BRL-TR-829; -215.

12. DISTRIBUTION/AVAILABILITY STATEMENT. Use agency-mandated availability statements to indicate the public availability or distribution limitations of the report. If additional limitations/ restrictions or special markings are indicated, follow agency authorization procedures, e.g. RD/FRD, PROPIN, ITAR, etc. Include copyright information.

13. SUPPLEMENTARY NOTES. Enter information not included elsewhere such as: prepared in cooperation with; translation of; report supersedes; old edition number, etc.

14. ABSTRACT. A brief (approximately 200 words) factual summary of the most significant information.

15. SUBJECT TERMS. Key words or phrases identifying major concepts in the report.

16. SECURITY CLASSIFICATION. Enter security classification in accordance with security classification regulations, e.g. U, C, S, etc. If this form contains classified information, stamp classification level on the top and bottom of this page.

17. LIMITATION OF ABSTRACT. This block must be completed to assign a distribution limitation to the abstract. Enter UU (Unclassified Unlimited) or SAR (Same as Report). An entry in this block is necessary if the abstract is to be limited.

Abstract

Two-mode nonlinear interaction (second-harmonic and second-subharmonic generation) in a planar waveguide with a small periodic corrugation at the surface is studied. Scattering of the interacting fields on the corrugation leads to field localization that enhances the nonlinear process provided that all the interactions are phase matched. Conditions for the overall phase matching are found. Compared with a perfectly quasi-phase matched waveguide, better values of squeezing as well as higher intensities are reached under these conditions. In pulsed regime, eigenmodes suitable for squeezed-light generation have been found.

I. INTRODUCTION

Since the pioneering work by Armstrong [1] on the process of second-harmonic generation has occurred, spatio-temporal properties of the nonlinearly interacting classical fields have been studied in detail by many authors both theoretically and experimentally. A new impulse in these studies has occurred when people understood that this process can give rise to the fields with nonclassical properties (for a review, see, e.g. [2–5]). Namely light with electric-field amplitude fluctuations suppressed below the limit given by quantum mechanics [6] can be generated both in the pump and second-subharmonic fields. Also light with nonclassical photon-number statistics can be obtained - pairwise character of photon-number statistics [7, 8] generated in the spontaneous process of second-subharmonic generation has been observed [9].

It has been shown that the best conditions for squeezed-light generation in homogeneous nonlinear media occur, provided that the nonlinear two-mode interaction is perfectly phase matched. Under these conditions, the principal squeeze variance of the second-subharmonic field can asymptotically reach zero when the gain of the nonlinear interaction increases. On the other hand, the pump-field principal squeeze variance cannot be less than 0.5 [10]. If large values of the nonlinear phase mismatch are allowed, this limit can be overcome due to a nonlinear phase modulation, as suggested in [11, 12]. However, the generated signal is very weak.

The most common method how to compensate for the natural nonlinear phase mismatch that occurs in commonly used nonlinear materials is to introduce an additional periodic modulation of the $\chi^{(2)}$ susceptibility using periodical poling [13–15]. Several methods for the additional modulation of the local amplitude of this quasi-phase-matched interaction have been developed [16]. These methods allow to reach a spectrally broad-band two-mode interaction and so femtosecond pumping of the nonlinear process is possible [17].

In order to effectively increase low values of the nonlinear interaction in real materials, configurations in which a nonlinear medium is put inside a cavity are usually used to generate squeezed light (e.g. [6, 18]).

In a waveguiding geometry that profits from a strong spatial localization of the interacting optical fields resulting in high values of the effective nonlinearity, another method to reach a nonlinear phase mismatch is possible. One of the nonlinearly interacting fields can be coupled through its evanescent waves into another field of the same frequency propagating in a neighbouring waveguide. An exchange of energy between these two linearly coupled fields introduces a spatial modulation of the nonlinearly interacting field that can be set to compensate for the nonlinear phase mismatch [19]. Interaction of fields in different waveguides through their evanescent waves can be used in various configurations that modify nonclassical properties of optical fields emerging from nonlinear interactions [20].

A waveguiding geometry allows another possibility to tailor the nonlinear process - a linear periodic corrugation of the waveguide surface can be introduced leading to scattering of the propagating fields [21, 22]. Spatial distributions of the electric-field amplitudes of the nonlinearly interacting fields are modified this way and higher conversion efficiencies of the nonlinear process can emerge [23, 24]. Also squeezed-light generation is supported in this geometry, as discussed in [25] where scattering of the second-harmonic field on the corrugation has been neglected. A waveguiding geometry with a periodic corrugation can also be conveniently used for second-harmonic generation in Čerenkov configuration [26]. A general model of squeezed-light generation in nonlinear photonic structures has been developed in [27].

In the pulsed regime and travelling-wave configuration, squeezed-light generation in the considered nonlinear interaction has been studied with the help of phase-space quasi-distributions or the corresponding Langevin stochastic equations [28]. It has also been shown that there exist correlations between intensities of the interacting fields in their transverse planes [29, 30]. A local oscillator in the form of an ultrashort optical pulse is needed to observe pulsed squeezing experimentally. The effort to observe the largest possible values of squeezing has raised the question about an optimum shape of the local-oscillator field [31, 32]. A general method how to solve this problem is to use the Bloch-Messiah reduction of the Green functions characterizing the linearized operator amplitude evolution [33]. This method has been elaborated in detail in [34, 35] for degenerate parametric down-conversion in a BBO crystal and also relation between the Bloch-Messiah reduction and Schmidt decomposition of a two-photon amplitude characterizing spontaneous parametric down-conversion has been found. Mode structure of nonclassical states arising from squeezed states after post-selection using on/off detectors has been analyzed in [36].

In this report, we show that scattering of the interacting fields caused by a linear periodic corrugation supports the generation of squeezed light in both the pump and second-subharmonic fields provided that at least one of the interacting fields is spatially localized as a conse-

quence of scattering. We note that spatial localization of optical fields in this case is weak in comparison with that occurring in layered photonic band-gap structures [37–39].

The report is organized as follows. In Sec. II, a quantum model of the nonlinear interaction including both Heisenberg equations for operator electric-field amplitudes and model of a generalized superposition of signal and noise are presented for cw pumping. Conditions for an efficient squeezed-light generation are derived in Sec. III. A detailed analysis of a waveguide made of LiNbO₃ is contained in Sec. IV considering cw pumping. Generalization of the model to the case of multi-mode fields is given in Sec. V. Assuming a linear corrugation present in the strong pump field and weak nonlinear interaction and relying on perturbation approach, eigenmodes of the generated pulsed second-subharmonic field are found in Sec. VI. Neglecting frequency dependence of the coupling constants and inter-mode dispersion, the corresponding equations for operator amplitudes are solved in Sec. VII. Numerical analysis of the principal squeeze variances of characteristic eigenmodes is contained in Sec. VIII. Conclusions are drawn in Sec. IX. Appendix A is devoted to mode analysis of an anisotropic planar waveguide. An optimum mode profile with respect to pulsed squeezing is found in Appendix B.

II. CW MODEL OF THE NONLINEAR INTERACTION

An overall electric-field amplitude $\mathbf{E}(\mathbf{r}, t)$ describing an optical field in the considered anisotropic nonlinear waveguide (shown in Fig. 1) [40] is composed of two contributions; pump (or fundamental) electric-field amplitude $\mathbf{E}_p(\mathbf{r}, t)$ at frequency ω and second-subharmonic electric-field amplitude $\mathbf{E}_s(\mathbf{r}, t)$ at frequency $\omega/2$; i.e. $\mathbf{E} = \mathbf{E}_p + \mathbf{E}_s$. We note that in case of second-harmonic generation, the field with the amplitude $\mathbf{E}_p(\mathbf{r}, t)$ is called second-harmonic and that with the amplitude $\mathbf{E}_s(\mathbf{r}, t)$ is known as pump. We keep the terminology used for second-subharmonic generation throughout the report. The electric-field amplitude \mathbf{E} obeys the wave equation inside the waveguide with a nonlinear source term [41]:

$$\Delta \mathbf{E} - \nabla(\nabla \cdot \mathbf{E}) - \mu \epsilon_0 \epsilon \cdot \frac{\partial^2 \mathbf{E}}{\partial t^2} = \mu \frac{\partial^2 \mathbf{P}_{nl}}{\partial t^2}. \quad (1)$$

In Eq. (1) μ denotes vacuum permeability, ϵ_0 vacuum permittivity, and \mathbf{P}_{nl} describes nonlinear polarization of the medium. The symbol Δ stands for Laplace operator, (\cdot) means a scalar product, and \cdot denotes tensorial multiplication. Every spectral component of the element $\epsilon_{ij}(\mathbf{r}, \omega)$ of the relative permittivity tensor in the considered waveguide can be expressed as follows:

$$\epsilon_{ij}(x, y, z, \omega) = \bar{\epsilon}_{ij}(x, y, \omega) [1 + \Delta \epsilon_{ij}(x, y, z, \omega)]. \quad (2)$$

Small variations of permittivity ϵ described by $\Delta \epsilon_{ij}(x, y, z, \omega)$ are induced by a periodic corrugation of

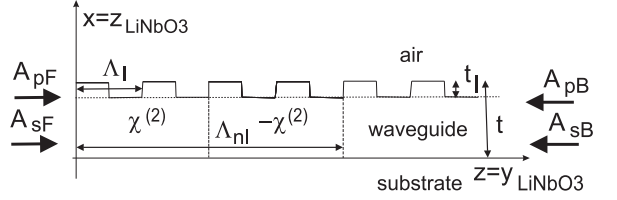


FIG. 1: Four optical fields interact in a nonlinear waveguide of thickness t and length L with a periodically-poled (period Λ_{nl}) $\chi^{(2)}$ susceptibility; A_{pF} , A_{pB} , A_{sF} , and A_{sB} mean forward-propagating pump, backward-propagating pump, forward-propagating second-subharmonic, and backward-propagating second-subharmonic electric-field amplitudes, respectively. A linear corrugation with depth t_l and period Λ_l is fabricated on the waveguide upper surface. Profile of the waveguide in the $x-y$ plane is rectangular with width Δy and depth t ; $\Delta y \gg t$ is assumed. The waveguide is made of LiNbO₃ with the optical axis oriented along the x axis.

the waveguide surface. These variations of the elements $\Delta \epsilon_{ij}(x, y, z, \omega)$ along the z axis can be conveniently decomposed into harmonic waves:

$$\Delta \epsilon_{ij}(x, y, z, \omega) = \sum_{q=-\infty}^{\infty} \epsilon_{ij,q}(x, y, \omega) \exp \left[i q \frac{2\pi}{\Lambda_l} z \right], \quad (3)$$

where $\epsilon_{q,ij}$ are coefficients of the decomposition and Λ_l is a period of the linear corrugation. Amplitude of the nonlinear polarization \mathbf{P}_{nl} of the medium is determined using tensor \mathbf{d} of the second-order nonlinear coefficient:

$$\mathbf{P}_{nl}(\mathbf{r}, t) = 2\epsilon_0 \mathbf{d}(\mathbf{r}) \cdot \mathbf{E}(\mathbf{r}, t) \mathbf{E}(\mathbf{r}, t). \quad (4)$$

Taking into account geometry of our waveguide elements $\mathbf{d}_{ijk}(\mathbf{r})$ of the nonlinear coefficient can be expressed as follows:

$$\mathbf{d}_{ijk}(x, y, z) = \sum_{q=-\infty}^{\infty} \mathbf{d}_{ijk,q}(x, y) \exp \left[i q \frac{2\pi}{\Lambda_{nl}} z \right], \quad (5)$$

where Λ_{nl} describes the period of a possible periodical poling of the nonlinear material.

The electric-field amplitudes of pump (\mathbf{E}_p) and second-subharmonic (\mathbf{E}_s) monochromatic waves can be expressed in the form:

$$\begin{aligned} \mathbf{E}_a(x, y, z, t) = & i [A_{aF}(z) \mathbf{e}_a(x, y) \exp(i\beta_a z - i\omega_a t) \\ & + A_{aB}(z) \mathbf{e}_a(x, y) \exp(-i\beta_a z - i\omega_a t) \\ & - \text{H.c.}], \quad a = p, s, \end{aligned} \quad (6)$$

where the symbols \mathbf{e}_p and \mathbf{e}_s refer to mode functions in the transverse plane of the beams. Amplitudes A_{pF} and A_{sF} [A_{pB} and A_{sB}] describe forward- [backward-] propagating pump and second-subharmonic fields and are such that the quantities $|A_{pF}|^2$, $|A_{pB}|^2$, $|A_{sF}|^2$, and $|A_{sB}|^2$ give directly the number of photons in these fields. Symbol β_a means a propagation constant along the z axis in

mode a whereas ω_a stands for frequency of this mode. Symbol H.c. replaces hermitian conjugated terms. We note that the considered anisotropic waveguide supports only TM guided modes; TE modes are not guided and thus do not contribute significantly to nonlinear interaction.

Mode functions \mathbf{e}_p and \mathbf{e}_s describe the transverse profiles of pump and second-subharmonic fields, respectively, and fulfill the following equations:

$$\begin{aligned} \nabla \times (\nabla \times [\mathbf{e}_a(x, y) \exp(\pm i\beta_a z - i\omega_a t)]) \\ - \frac{\omega_a^2}{c^2} \bar{\epsilon}_{ij}(x, y, \omega_a) \cdot [\mathbf{e}_a(x, y) \exp(\pm i\beta_a z - i\omega_a t)] = 0, \\ a = p, s. \end{aligned} \quad (7)$$

We note that mean values of permittivities $\bar{\epsilon}_{ij}(x, y, \omega_a)$ are used for the determination of mode functions. The mode functions \mathbf{e}_p and \mathbf{e}_s are normalized to describe one photon in a mode inside the waveguide (see Appendix A).

Substitution of Eqs. (2-6) into Eq. (1) assuming $\left| \frac{\partial^2 A_{ab}}{\partial z^2} \right| \ll \left| \beta_a \frac{\partial A_{ab}}{\partial z} \right|$ for $a = p, s$ and $b = F, B$ (analog of the slowly-varying envelope approximation to spatial evolution) results in the following equations for amplitudes A_{pF} , A_{pB} , A_{sF} , and A_{sB} :

$$\begin{aligned} \frac{dA_{sF}}{dz} &= iK_s \exp(-i\delta_s z) A_{sB} \\ &\quad + 4K_{nl,q} \exp(i\delta_{nl,q} z) A_{pF} A_{sF}^*, \\ \frac{dA_{sB}}{dz} &= -iK_s^* \exp(i\delta_s z) A_{sF} \\ &\quad - 4K_{nl,q} \exp(-i\delta_{nl,q} z) A_{pB} A_{sB}^*, \\ \frac{dA_{pF}}{dz} &= iK_p \exp(-i\delta_p z) A_{pB} \\ &\quad - 2K_{nl,q}^* \exp(-i\delta_{nl,q} z) A_{sF}^2, \\ \frac{dA_{pB}}{dz} &= -iK_p^* \exp(i\delta_p z) A_{pF} \\ &\quad + 2K_{nl,q}^* \exp(i\delta_{nl,q} z) A_{sB}^2. \end{aligned} \quad (8)$$

Because the waveguide is made of an anisotropic material, also the following relation has to hold in order to derive correctly equations in Eq. (8) (for details, see [41]):

$$\begin{aligned} \frac{d^2 A_{ab}(z)}{dz^2} [\mathbf{e}_a(x, y)]_z \exp(\pm i\beta_a z) \mathbf{z} \\ + \frac{dA_{ab}(z)}{dz} \nabla ([\mathbf{e}_a(x, y)]_z \exp(\pm i\beta_a z)) \\ + \frac{dA_{ab}(z)}{dz} (\nabla \cdot [\mathbf{e}_a(x, y) \exp(\pm i\beta_a z)]) \mathbf{z} \approx 0, \\ a = p, s, \quad b = F, B, \end{aligned} \quad (9)$$

and \mathbf{z} stands for a unit vector along the z axis. We note that Eqs. (8) describe also a nonlinear coupler composed of two waveguides made of $\chi^{(2)}$ media whose modes interact through evanescent waves. Nonclassical properties of light propagating in this coupler have been studied in

[42, 43]. A scheme that allows to decompose interactions in this coupler into a sequence of fictitious interactions has been suggested in [44].

Phase mismatches δ_s , δ_p , and $\delta_{nl,q}$ occurring in Eq. (8) are given as follows:

$$\begin{aligned} \delta_a &= 2\beta_a - \frac{2\pi}{\Lambda_l}, \quad a = p, s, \\ \delta_{nl,q} &= \beta_p - 2\beta_s + q \frac{2\pi}{\Lambda_{nl}}. \end{aligned} \quad (10)$$

Coefficient q equals ± 1 for a periodically poled nonlinear material, whereas $q = 0$ for a material without periodic poling. Linear coupling constants K_p and K_s are determined along the expressions:

$$\begin{aligned} K_a &= \frac{\omega_a^2}{2c^2 \beta_a} \frac{\int dxdy \varepsilon_1(x, y, \omega_a) \cdot \mathbf{e}_a^*(x, y) \mathbf{e}_a(x, y)}{\int dxdy |\mathbf{e}_a(x, y)|^2}, \\ a &= p, s. \end{aligned} \quad (11)$$

Similarly, the following expression can be found for nonlinear coupling constants $K_{nl,q}$ for $q = 0, \pm 1$:

$$\begin{aligned} K_{nl,q} &= \frac{2i\omega_s^2}{c^2 \beta_s} \frac{\int dxdy \mathbf{d}_q(x, y) \cdot \mathbf{e}_p(x, y) \mathbf{e}_s^*(x, y) \mathbf{e}_s^*(x, y)}{\int dxdy |\mathbf{e}_s(x, y)|^2} \\ &\approx \frac{2i\omega_p^2}{c^2 \beta_p} \frac{\int dxdy \mathbf{d}_q(x, y) \cdot \mathbf{e}_p(x, y) \mathbf{e}_s^*(x, y) \mathbf{e}_s^*(x, y)}{\int dxdy |\mathbf{e}_p(x, y)|^2}. \end{aligned} \quad (12)$$

The last approximate equality in Eq. (12) is valid provided that $\omega_s/\beta_s \approx \omega_p/\beta_p$ and due to the normalization of the mode functions \mathbf{e}_s and \mathbf{e}_p . This approximation assures, that only one nonlinear coupling constant occurs in Eqs. (8) which is important in quantum description.

Expressions for linear (K_s , K_p) and nonlinear ($K_{nl,0}$, $K_{nl,1}$) coupling constants appropriate for the considered waveguide and derived from Eqs. (11) and (12) can be found in Appendix A in Eqs. (A10-A12).

Quantum model of the nonlinear interaction in the considered waveguide can be formulated changing the classical envelope electric-field amplitudes A_{pF} , A_{pB} , A_{sF} , and A_{sB} occurring in Eq. (6) into operators denoted as \hat{A}_{pF} , \hat{A}_{pB} , \hat{A}_{sF} , and \hat{A}_{sB} , respectively. A quantum analog of the classical equations written in Eq. (8) can then be derived from the Heisenberg equations (for details, see [45, 46];

$$\frac{d\hat{X}}{dz} = -\frac{i}{\hbar} [\hat{G}, \hat{X}]; \quad (13)$$

considering the following momentum operator \hat{G} :

$$\begin{aligned} \hat{G} &= \left[\hbar K_s \exp(-i\delta_s z) \hat{A}_{sF}^\dagger \hat{A}_{sB} \right. \\ &\quad \left. + \hbar K_p \exp(-i\delta_p z) \hat{A}_{pF}^\dagger \hat{A}_{pB} + \text{H.c.} \right] \\ &\quad - \left[2i\hbar K_{nl,q} \exp(i\delta_{nl,q} z) \hat{A}_{sF}^{\dagger 2} \hat{A}_{pF} \right. \\ &\quad \left. + 2i\hbar K_{nl,q} \exp(-i\delta_{nl,q} z) \hat{A}_{sB}^{\dagger 2} \hat{A}_{pB} + \text{H.c.} \right], \end{aligned} \quad (14)$$

where $q = 0$ or $q = \pm 1$. In Eq. (13), \hbar means the reduced Planck constant, \hat{X} stands for an arbitrary operator and symbol $[\cdot, \cdot]$ denotes commutator.

The operator quantum equations analogous to those written in Eq. (8) can be solved using the method of a small operator correction (denoted as $\delta\hat{A}$) to a mean value (denoted as A) in which an electric-field operator amplitude \hat{A} is decomposed as $\hat{A} = A + \delta\hat{A}$. This method provides a set of classical nonlinear equations for the mean values A that coincides with the set given in Eq. (8). The operator electric-field amplitude corrections $\delta\hat{A}$ fulfill the following linear operator equations:

$$\begin{aligned}\frac{d\delta\hat{A}_{s_F}}{dz} &= \mathcal{K}_s\delta\hat{A}_{s_B} + \mathcal{K}_{F,q} \left[A_{p_F}\delta\hat{A}_{s_F}^\dagger + A_{s_F}^*\delta\hat{A}_{p_F} \right], \\ \frac{d\delta\hat{A}_{s_B}}{dz} &= \mathcal{K}_s^*\delta\hat{A}_{s_F} - \mathcal{K}_{B,q} \left[A_{p_B}\delta\hat{A}_{s_B}^* + A_{s_B}^*\delta\hat{A}_{p_B} \right], \\ \frac{d\delta\hat{A}_{p_F}}{dz} &= \mathcal{K}_p\delta\hat{A}_{p_B} - \mathcal{K}_{F,q}^*A_{s_F}\delta\hat{A}_{s_F}, \\ \frac{d\delta\hat{A}_{p_B}}{dz} &= \mathcal{K}_p^*\delta\hat{A}_{p_B} + \mathcal{K}_{B,q}^*A_{s_B}\delta\hat{A}_{s_B}.\end{aligned}\quad (15)$$

Functions \mathcal{K}_s , \mathcal{K}_p , and $\mathcal{K}_{nl,q}$ introduced in Eqs. (15) are defined as:

$$\begin{aligned}\mathcal{K}_a &= iK_a \exp(-i\delta_a z), \quad a = s, p, \\ \mathcal{K}_{F,q} &= 4K_{nl,q} \exp(i\delta_{nl,q} z), \\ \mathcal{K}_{B,q} &= 4K_{nl,q} \exp(-i\delta_{nl,q} z).\end{aligned}\quad (16)$$

Solution of the classical nonlinear equations written in Eqs. (8) can only be reached numerically using, e.g., a finite difference method called BVP [47]. This method requires an initial guess of the solution that can be conveniently obtained when the nonlinear terms in Eqs. (8) are omitted. Then, the initial solution can be written as follows:

$$\begin{aligned}A_{a_F}^{(0)} &= \exp\left(-i\frac{\delta_a z}{2}\right) \left[B_a \cos(\Delta_a z) + \tilde{B}_a \sin(\Delta_a z) \right], \\ A_{a_B}^{(0)} &= \exp\left(i\frac{\delta_a z}{2}\right) \\ &\times \left[B_a \left(-\frac{\delta_a}{2K_a} \cos(\Delta_a z) + i\frac{\Delta_a}{K_a} \sin(\Delta_a z) \right) \right. \\ &\left. + \tilde{B}_a \left(-\frac{\delta_a}{2K_a} \sin(\Delta_a z) - i\frac{\Delta_a}{K_a} \cos(\Delta_a z) \right) \right], \\ a &= s, p,\end{aligned}\quad (17)$$

and

$$\Delta_a = \sqrt{\frac{\delta_a^2}{4} - |K_a|^2}, \quad a = s, p. \quad (18)$$

In Eqs. (17), constants B_p , \tilde{B}_p , B_s , and \tilde{B}_s are set according to the boundary conditions at both sides of the waveguide.

We note that any solution of the nonlinear equations in Eqs. (8) obeys the following relation useful in a numerical computation:

$$\frac{d}{dz} (|A_{s_F}|^2 + 2|A_{p_F}|^2 - |A_{s_B}|^2 - 2|A_{p_B}|^2) = 0. \quad (19)$$

The solution of the system of linear operator equations in Eqs. (15) for the operator electric-field amplitude corrections $\delta\hat{A}$ can be found numerically and put into the following matrix form:

$$\begin{pmatrix} \delta\hat{A}_{F,\text{out}} \\ \delta\hat{A}_{B,\text{in}} \end{pmatrix} = \begin{pmatrix} \mathcal{U}_{FF} & \mathcal{U}_{FB} \\ \mathcal{U}_{BF} & \mathcal{U}_{BB} \end{pmatrix} \begin{pmatrix} \delta\hat{A}_{F,\text{in}} \\ \delta\hat{A}_{B,\text{out}} \end{pmatrix}, \quad (20)$$

where

$$\begin{aligned}\delta\hat{A}_{F,\text{in}} &= \begin{pmatrix} \delta\hat{A}_{s_F}(0) \\ \delta\hat{A}_{s_F}^\dagger(0) \\ \delta\hat{A}_{p_F}(0) \\ \delta\hat{A}_{p_F}^\dagger(0) \end{pmatrix}, \quad \delta\hat{A}_{F,\text{out}} = \begin{pmatrix} \delta\hat{A}_{s_F}(L) \\ \delta\hat{A}_{s_F}^\dagger(L) \\ \delta\hat{A}_{p_F}(L) \\ \delta\hat{A}_{p_F}^\dagger(L) \end{pmatrix}, \\ \delta\hat{A}_{B,\text{in}} &= \begin{pmatrix} \delta\hat{A}_{s_B}(L) \\ \delta\hat{A}_{s_B}^\dagger(L) \\ \delta\hat{A}_{p_B}(L) \\ \delta\hat{A}_{p_B}^\dagger(L) \end{pmatrix}, \quad \delta\hat{A}_{B,\text{out}} = \begin{pmatrix} \delta\hat{A}_{s_B}(0) \\ \delta\hat{A}_{s_B}^\dagger(0) \\ \delta\hat{A}_{p_B}(0) \\ \delta\hat{A}_{p_B}^\dagger(0) \end{pmatrix}\end{aligned}\quad (21)$$

and L means length of the waveguide. Matrices \mathcal{U}_{FF} , \mathcal{U}_{FB} , \mathcal{U}_{BF} , and \mathcal{U}_{BB} are determined using numerical solution of Eqs. (15).

The following input-output relations among the operator amplitude corrections $\delta\hat{A}$,

$$\begin{pmatrix} \delta\hat{A}_{F,\text{out}} \\ \delta\hat{A}_{B,\text{out}} \end{pmatrix} = \begin{pmatrix} \mathcal{U}_{FF} - \mathcal{U}_{FB}\mathcal{U}_{BB}^{-1}\mathcal{U}_{BF} & \mathcal{U}_{FB}\mathcal{U}_{BB}^{-1} \\ -\mathcal{U}_{BB}^{-1}\mathcal{U}_{BF} & \mathcal{U}_{BB}^{-1} \end{pmatrix} \times \begin{pmatrix} \delta\hat{A}_{F,\text{in}} \\ \delta\hat{A}_{B,\text{in}} \end{pmatrix} \quad (22)$$

$$= \mathcal{U} \begin{pmatrix} \delta\hat{A}_{F,\text{in}} \\ \delta\hat{A}_{B,\text{in}} \end{pmatrix}, \quad (23)$$

are found solving Eqs. (21) with respect to vectors $\delta\hat{A}_{F,\text{out}}$ and $\delta\hat{A}_{B,\text{out}}$. The output operator electric-field amplitude corrections contained in vectors $\delta\hat{A}_{F,\text{out}}$ and $\delta\hat{A}_{B,\text{out}}$ obey boson commutation relations provided that the input operator electric-field amplitude corrections given in vectors $\delta\hat{A}_{F,\text{in}}$ and $\delta\hat{A}_{B,\text{in}}$ are ruled by boson commutation relations. We note that also certain commutation relations among the operator electric-field amplitude corrections in vectors $\delta\hat{A}_{F,\text{out}}$ and $\delta\hat{A}_{B,\text{in}}$ can be derived (for details, see [46]).

We restrict our considerations to states of optical fields that can be described using the generalized superposition of signal and noise [2]. Thus coherent states, squeezed states as well as noise can be considered. Parameters B_j , C_j , D_{jk} , and \tilde{D}_{jk} defined below are sufficient for the description of any state of a two-mode optical field in this approximation [20]:

$$B_j = \langle \Delta\hat{A}_j^\dagger \Delta\hat{A}_j \rangle,$$

$$\begin{aligned}
C_j &= \langle (\Delta \hat{A}_j)^2 \rangle, \\
D_{jk} &= \langle \Delta \hat{A}_j \Delta \hat{A}_k \rangle, \quad j \neq k, \\
\bar{D}_{jk} &= -\langle \Delta \hat{A}_j^\dagger \Delta \hat{A}_k \rangle, \quad j \neq k;
\end{aligned} \quad (24)$$

$\Delta \hat{A}_j = \hat{A}_j - \langle \hat{A}_j \rangle$; symbol $\langle \rangle$ denotes the quantum statistical mean value. Expressions for the coefficients B_j , C_j , D_{jk} , and \bar{D}_{jk} appropriate for outgoing fields can be derived [46] using elements of matrix \mathcal{U} given in Eq. (23) and incident values of coefficients $B_{j,\text{in},\mathcal{A}}$ and $C_{j,\text{in},\mathcal{A}}$ related to anti-normal ordering of field operators (for details, see [20]):

$$\begin{aligned}
B_{j,\text{in},\mathcal{A}} &= \cosh^2(r_j) + n_{ch,j}, \\
C_{j,\text{in},\mathcal{A}} &= \frac{1}{2} \exp(i\vartheta_j) \sinh(2r_j).
\end{aligned} \quad (25)$$

In Eq. (25), r_j stands for a squeeze parameter of the incident j -th field, ϑ_j means a squeeze phase, and $n_{ch,j}$ stands for a mean number of incident chaotic photons. Coefficients $D_{jk,\text{in},\mathcal{A}}$ and $\bar{D}_{jk,\text{in},\mathcal{A}}$ for an incident field are considered to be zero, i.e. the incident fields are assumed to be statistically independent.

The maximum attainable value of squeezing of electric-field amplitude fluctuations is given by the value of a principal squeeze variance λ [2]. Both single-mode principal squeeze variances λ_j and compound-mode principal squeeze variances λ_{ij} (characterizing an overall field composed of two other fields) can be determined in terms of coefficients B_j , C_j , D_{jk} , and \bar{D}_{jk} given in Eq. (24) (for details, see, [2, 20]):

$$\lambda_j = 1 + 2[B_j - |C_j|], \quad (26)$$

$$\begin{aligned}
\lambda_{jk} &= 2[1 + B_j + B_k - 2\Re(\bar{D}_{jk}) \\
&\quad - |C_j + C_k + 2D_{jk}|];
\end{aligned} \quad (27)$$

symbol \Re means the real part of an expression. Values of the principal squeeze variance λ_j (λ_{jk}) less than one (two) indicate squeezing in a single-mode (compound-mode) case.

III. SUITABLE CONDITIONS FOR SQUEEZED-LIGHT GENERATION

It occurs that there exist two conditions for an efficient squeezed-light generation. The first condition comes from the requirement that the nonlinear interaction should be phase-matched along the whole waveguide, whereas the second one gives optimum conditions for the localization of interacting optical fields.

A. Overall phase-matching of the nonlinearly interacting fields

Conditions for an optimum phase-matching of the interacting fields can be revealed, when we write the differential equation for the number N_a of photons in field

a ; $N_a = A_a^* A_a$. Using Eqs. (8) we arrive at the following differential equations:

$$\begin{aligned}
\frac{dN_{s_F}}{dz} &= -2\Im \{ K_s \exp(-i\delta_s z) A_{s_F}^* A_{s_B} \} \\
&\quad + 8\Re \{ K_{nl,q} \exp(i\delta_{nl,q} z) A_{s_F}^{*2} A_{p_F} \}, \\
\frac{dN_{s_B}}{dz} &= -2\Im \{ K_s \exp(-i\delta_s z) A_{s_F}^* A_{s_B} \} \\
&\quad - 8\Re \{ K_{nl,q} \exp(-i\delta_{nl,q} z) A_{s_B}^{*2} A_{p_B} \}, \\
\frac{dN_{p_F}}{dz} &= -2\Im \{ K_p \exp(-i\delta_p z) A_{p_F}^* A_{p_B} \} \\
&\quad - 4\Re \{ K_{nl,q} \exp(i\delta_{nl,q} z) A_{s_F}^{*2} A_{p_F} \}, \\
\frac{dN_{p_B}}{dz} &= -2\Im \{ K_p \exp(-i\delta_p z) A_{p_F}^* A_{p_B} \} \\
&\quad + 4\Re \{ K_{nl,q} \exp(-i\delta_{nl,q} z) A_{s_B}^{*2} A_{p_B} \};
\end{aligned} \quad (28)$$

symbol \Im denotes the imaginary part of an expression. We note that the first terms on the right-hand side of the first and the second (as well as the third and the fourth) equations in Eqs. (28) have the same sign because of counter-propagation of the fields [see also Eq. (19)]. The nonlinear interaction described by the second terms on the right-hand sides of Eqs. (28) is weak and so we can judge the contribution of these terms using a perturbation approach. In the first step we neglect the nonlinear terms in Eqs. (8) and solve Eqs. (8) for field amplitudes $A_{s_F}^{(0)}$, $A_{s_B}^{(0)}$, $A_{p_F}^{(0)}$, and $A_{p_B}^{(0)}$. Then we insert this solution into the nonlinear terms in Eqs. (28) and find this way optimum conditions that maximize contributions of these terms. The solution for amplitudes $A_{s_F}^{(0)}$, $A_{s_B}^{(0)}$, $A_{p_F}^{(0)}$, and $A_{p_B}^{(0)}$ coincides with that written in Eqs. (17) as an initial guess for numerical solution and we rewrite it into the following suitable form:

$$\begin{aligned}
A_{a_F}^{(0)}(z) &= \exp\left(-i\frac{\delta_a z}{2}\right) \\
&\quad \times [\mathcal{B}_{a_F}^+ \exp(i\Delta_a z) + \mathcal{B}_{a_F}^- \exp(-i\Delta_a z)], \\
\mathcal{B}_{a_F}^+ &= \frac{B_a - i\tilde{B}_a}{2}, \\
\mathcal{B}_{a_F}^- &= \frac{B_a + i\tilde{B}_a}{2}, \\
A_{a_B}^{(0)}(z) &= \exp\left(i\frac{\delta_a z}{2}\right) \\
&\quad \times [\mathcal{B}_{a_B}^+ \exp(i\Delta_a z) + \mathcal{B}_{a_B}^- \exp(-i\Delta_a z)], \\
\mathcal{B}_{a_B}^+ &= \frac{-\delta_a + 2\Delta_a}{4K_a} (B_a - i\tilde{B}_a), \\
\mathcal{B}_{a_B}^- &= \frac{-\delta_a - 2\Delta_a}{4K_a} (B_a + i\tilde{B}_a), \quad a = p, s.
\end{aligned} \quad (29)$$

Provided that a linear corrugation is missing in field a the solution for amplitudes $A_{a_F}^{(0)}$ and $A_{a_B}^{(0)}$ can be obtained from the expressions in Eqs. (29) using a sequence of two limits; $\delta_a \rightarrow 0$, $K_a \rightarrow 0$:

$$A_{a_F}^{(0)}(z) = B_a,$$

$$A_{aB}^{(0)}(z) = \tilde{B}_a. \quad (30)$$

Interaction between the forward-propagating fields is described in Eqs. (28) in our perturbation approach by the term

$$\Re \left\{ K_{nl,q} \exp(i\delta_{nl,q}z) A_{s_F}^{(0)*2} A_{p_F}^{(0)} \right\} \quad (31)$$

that, after substituting the expressions for amplitudes $A_{s_F}^{(0)}$ and $A_{p_F}^{(0)}$ from Eqs. (29), splits into the following eight terms:

$$\Re \left\{ K_{nl,q} \mathcal{B}_{s_F}^{\pm*} \mathcal{B}_{s_F}^{\pm*} \mathcal{B}_{p_F}^{\pm} \right. \\ \left. \times \exp(i[\delta_{nl,q} + \delta_s - \delta_p/2 \mp \Delta_s \mp \Delta_s \pm \Delta_p]z) \right\}. \quad (32)$$

The nonlinear interaction is efficient under the condition that one of these terms does not oscillate along the z axis. This gives us eight possible conditions that combine nonlinear phase-mismatch $\delta_{nl,q}$ and parameters of the corrugation δ_s , δ_p , K_s , and K_p :

$$\delta_{nl,q} + \delta_s - \delta_p/2 \mp \Delta_s \mp \Delta_s \pm \Delta_p = 0. \quad (33)$$

It depends on a given waveguide and initial conditions which out of these eight conditions leads to an efficient nonlinear interaction. We note that the conditions in Eq. (33) are valid also for the nonlinear interaction between the backward-propagating fields characterized by the term $\Re \left\{ K_{nl,q} \exp(-i\delta_{nl,q}z) A_{s_B}^{(0)*2} A_{p_B}^{(0)} \right\}$ in Eqs. (28).

We consider two special cases in which a linear corrugation is present either in the pump or the second-subharmonic field. Assuming the linear corrugation in the pump field the conditions in Eq. (33) get the form:

$$\delta_{nl,q} - \delta_p/2 \pm \Delta_p = 0. \quad (34)$$

Sign - (+) is suitable for $\delta_{nl,q} > 0$ ($\delta_{nl,q} < 0$) when we solve Eq. (34) for δ_p :

$$\delta_p = \delta_{nl,q} + \frac{|K_p|^2}{\delta_{nl,q}}; \quad (35)$$

i.e. $\delta_{nl,q}$ and δ_p have the same sign. The expression in Eq. (35) then determines the period Λ_l of linear corrugation:

$$\Lambda_l = \frac{\pi}{\beta_p - \delta_{nl,q}/2 - |K_p|^2/(2\delta_{nl,q})}. \quad (36)$$

On the other hand, the conditions

$$\delta_{nl,q} + \delta_s/2 \mp \Delta_s \mp \Delta_s = 0 \quad (37)$$

are suitable for the linear corrugation in the second-subharmonic field. When $\delta_{nl,q} > 0$ ($\delta_{nl,q} < 0$) signs - (+) in Eq. (37) are appropriate and we have:

$$\delta_s = -\frac{\delta_{nl,q}}{2} - \frac{2|K_s|^2}{\delta_{nl,q}}; \quad (38)$$

i.e. $\delta_{nl,q}$ and δ_s have opposite signs. The period Λ_l of linear corrugation is then given as

$$\Lambda_l = \frac{\pi}{\beta_s + \delta_{nl,q}/4 + |K_p|^2/\delta_{nl,q}}. \quad (39)$$

B. Localization of the interacting fields

If we have considered a waveguide with the linear corrugation so deep that it touches the bottom of the waveguide, we would have a layered structure with band-gaps and transmission peaks. If a field frequency lies in a transmission peak, the field is also well localized inside the structure [37]. The considered waveguide with a weak linear corrugation behaves qualitatively in the same way [23]. The areas of transparency of the waveguide are convenient for the nonlinear interaction because of the field localization (though very weak for a weak corrugation). A transmission peak of the waveguide can be found from the condition that a backward-propagating field is zero both at the beginning and at the end of the waveguide, because it is not initially seeded. These requirements are fulfilled by the solution in Eqs. (17) under the following conditions:

$$\Delta_a = \frac{m\pi}{L}, \quad m = 1, 2, \dots; \\ B_a = A_{a_F}^{(0)}(0); \quad \tilde{B}_a = \frac{i\delta_a}{2\Delta_a} B_a, \quad a = p, s. \quad (40)$$

Natural number m counts areas of transmission.

The linear phase mismatch δ_a is determined from the first equation in Eqs. (40) in the following form

$$\delta_a = \pm 2\sqrt{\left(\frac{m\pi}{L}\right)^2 + |K_a|^2}, \quad a = p, s, \quad (41)$$

and the corresponding period Λ_l of linear corrugation is given as:

$$\Lambda_l = \frac{\pi}{\beta_a \pm \sqrt{(m\pi/L)^2 + |K_a|^2}}. \quad (42)$$

The conditions in Eqs. (35) and (41) for a linear corrugation in the pump field can be combined together to provide the following formula for the coupling constant K_p :

$$|K_p|^2 = \delta_{nl,q}^2 \left(1 \pm \frac{2m\pi}{|\delta_{nl,q}|L} \right). \quad (43)$$

The linear phase mismatch δ_p is then determined along the formula in Eq. (41) such that the signs of $\delta_{nl,q}$ and δ_p are the same.

Similarly the conditions for a linear corrugation in the second-subharmonic field written in Eqs. (38) and (41) and considered together lead to an expression for the coupling constant K_s :

$$|K_s|^2 = \frac{\delta_{nl,q}^2}{4} \left(1 \pm \frac{4m\pi}{|\delta_{nl,q}|L} \right). \quad (44)$$

The sign of linear phase mismatch δ_s determined from Eq. (41) is opposite to that of $\delta_{nl,q}$.

IV. SQUEEZED-LIGHT GENERATION - NUMERICAL ANALYSIS FOR CW PUMPING

Discussion of squeezed-light generation is decomposed into three parts. In the first one, we pay a detailed attention to attainable characteristics of the considered waveguide. The second part is devoted to second-subharmonic generation, i.e. an incident strong pump field is assumed. In the third part, a strong incident second-subharmonic field is assumed, i.e. second-harmonic generation is studied.

A. Characteristic parameters of the waveguide

We consider a waveguide made of LiNbO₃ with length $L = 1 \times 10^{-3}$ m and width $\Delta y = 1 \times 10^{-5}$ m pumped at the wavelength $\lambda_p = 0.534 \times 10^{-6}$ m ($\lambda_s = 1.064 \times 10^{-6}$ m). More details are contained in Appendix A. We require a single-mode operation at both the pump- and second-subharmonic-field frequencies that can be achieved for the thickness t of the waveguide in the range $t \in (0.403, 0.544) \times 10^{-6}$ m [24]. We also neglect losses in the waveguide that may be caused both by absorption inside the waveguide and scattering of light that does not propagate into guided modes.

Values of the natural nonlinear phase mismatch $\delta_{nl,0}$ are high (around 1.7×10^6 m⁻¹) in the region of single-mode operation and depend on the thickness t of the waveguide (see Fig. 2a). Values of the nonlinear coupling constant $K_{nl,0}$ depicted in Fig. 2b increase with the increasing values of the thickness t because of the thicker the waveguide the more the modes are localized inside the waveguide and so the greater the overlap of the nonlinearly interacting field amplitudes. Attainable values of linear coupling constants K_p and K_s for different values of thickness t and depth of corrugation t_l can be obtained from Fig. 3. Values of the coupling constants K_p and K_s for a given thickness t increase monotonously with the increasing values of the depth of corrugation t_l . For small values of the thickness t , values of the coupling constant K_s are small because the waveguide is thin for the second-subharmonic field and so a considerable part of the field is outside the waveguide and cannot be scattered by the corrugation.

Amplitudes of the dimensionless incident strong electric-field amplitudes A_{ab} are determined from the incident power P_{ab} along the relation:

$$|A_{ab}| = \sqrt{\frac{P_{ab} L \beta_a}{\hbar \omega_a^2}}, \quad a = p, s, \quad b = F, B. \quad (45)$$

On the other hand, power P_{ab}^{out} of an outgoing field is given as follows:

$$P_{ab}^{\text{out}} = \frac{\hbar \omega_a^2}{\beta_a L} |A_{ab}|^2$$

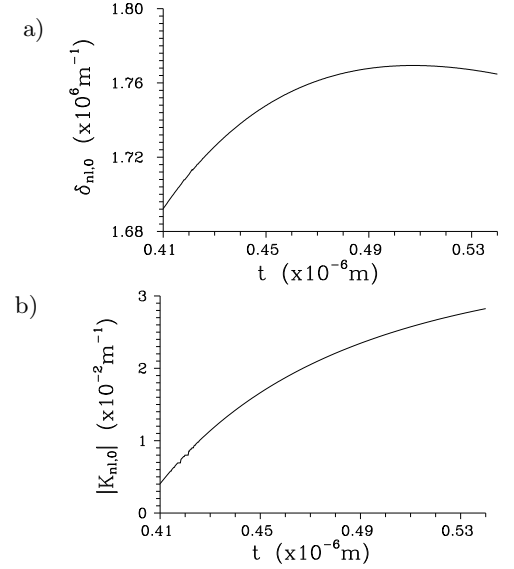


FIG. 2: Natural nonlinear phase mismatch $\delta_{nl,0}$ (a) and absolute value of the nonlinear coupling constant $K_{nl,0}$ (b) as they depend on the thickness t of the waveguide are shown in the region of single-mode operation; constant $K_{nl,0}$ is determined for amplitudes that correspond to one pump and one second-subharmonic photon inside the waveguide.

$$= \frac{\hbar \omega_a^2}{\beta_a L} N_{ab}, \quad a = p, s, \quad b = F, B; \quad (46)$$

N_{ab} denotes the number of photons leaving the waveguide.

New dimensionless parameters are convenient for the discussion of behavior of the waveguide;

$$\begin{aligned} z^r &= z/L, \\ \Lambda_l^r &= \Lambda_l/L, \Lambda_{nl,q}^r = \Lambda_{nl,q}/L, \\ \beta_a^r &= L\beta_a, \delta_a^r = L\delta_a, K_a^r = LK_a, \quad a = p, s, \\ \delta_{nl,q}^r &= L\delta_{nl,q}, K_{nl,q}^r = LK_{nl,q}. \end{aligned} \quad (47)$$

Applying these parameters the waveguide extends from $z^r = 0$ to $z^r = 1$. The dimensionless parameters enable to understand the behavior of the waveguide as it depends on the length L using graphs and discussion below.

B. Second-subharmonic generation

As a reference for the efficiency of squeezed-light generation we consider the waveguide with periodical poling and assume that it is pumped by the power of 2 W. The nonlinear interaction is perfectly phase matched for the period of poling $\Lambda_{nl}^r \approx 3.552 \times 10^{-3}$ where we have for the principal squeeze variances $\lambda_{s_F} \approx 0.45$ and $\lambda_{p_F} \approx 1$ (see Fig. 4a). The more distant the value of Λ_{nl}^r from the above-mentioned optimum value is, the larger the nonlinear phase mismatch and the larger the value of the principal squeeze variance λ_{s_F} .

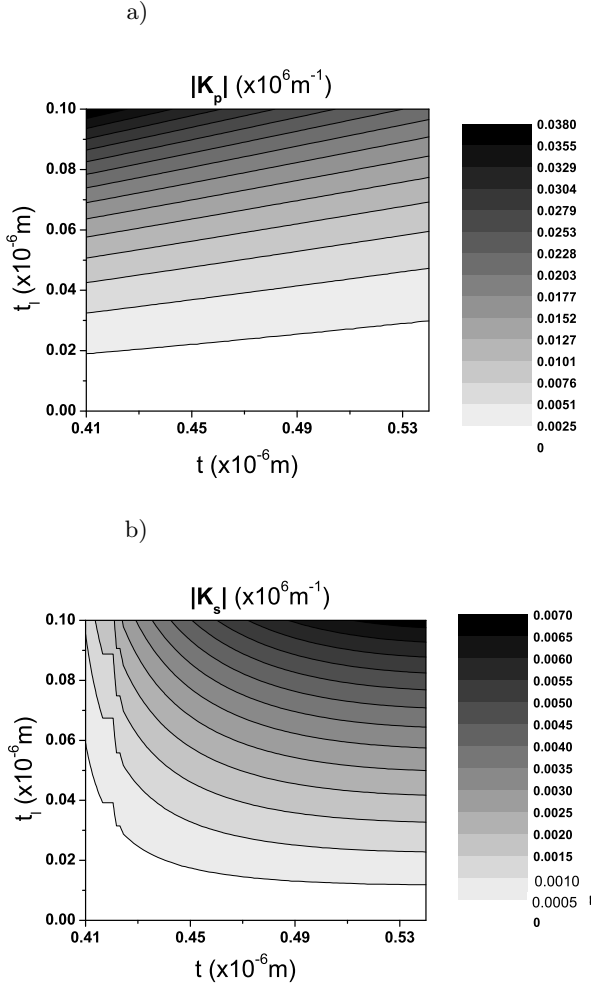


FIG. 3: Contour plot of the absolute value of pump-field [second-subharmonic-field] linear coupling constant K_p [K_s] as it depends on thickness t of the waveguide and depth t_l of linear corrugation is shown in (a) [(b)] in the region of single-mode operation.

Considering a periodic corrugation in the pump field, better values of squeezing in the second-subharmonic field can be reached. The reason is that the corrugation causes scattering of the pump field that leads to inhomogeneity of the field along the z axis. The nonlinear process then profits from field localization. However, nonzero values of the nonlinear phase mismatch $\delta_{nl,1}$ are important to exploit this localization because they have to compensate periodic spatial oscillations caused by the corrugation (see [48]). A perfect phase matching of all the processes occurring in the waveguide can be reached this way.

A typical dependence of the principal squeeze variance λ_{s_F} as well as the number N_{s_F} of photons leaving the waveguide for the forward-propagating second-subharmonic field for attainable values of parameters of

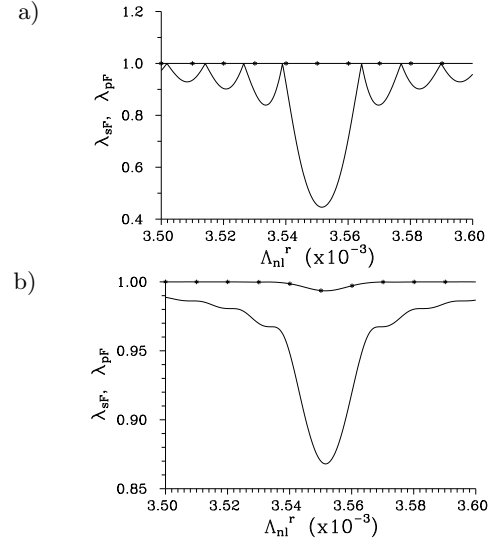


FIG. 4: Principal squeeze variances λ_{s_F} (solid curve) and λ_{p_F} (solid curve with $*$) as functions of the period Λ_{nl}^r of poling for second-subharmonic generation ($P_{p_F} = 2$ W, $P_{s_F} = 1 \times 10^{-10}$ W - a negligible seeding to substitute spontaneous process in classical equations) (a) and second-harmonic generation ($P_{p_F} = 1 \times 10^{-10}$ W, $P_{s_F} = 2$ W) (b); to understand the behavior with respect to the length L , the period Λ_{nl} should be decomposed as $\Lambda_{nl}^0 + \Delta\Lambda_{nl}$, then $\delta_{nl,q}^r \approx -2\pi q \Delta\Lambda_{nl}^r / \Lambda_{nl}^0{}^2$, $\Lambda_{nl}^0 = 2\pi q / (2\beta_s - \beta_p)$, $\Delta\Lambda_{nl}^r = L\Delta\Lambda_{nl}$; $t = 5 \times 10^{-7}$ m, $K_p^r = 0$, $K_s^r = 0$, $\arg(A_{p_F}) = 0$, $\arg(A_{s_F}) = 0$, $A_{p_B} = 0$, $A_{s_B} = 0$; $\Lambda_{nl}^0 \approx 3.552 \times 10^{-6}$ m.

the corrugation is shown in Fig. 5 assuming a fixed value of the nonlinear phase mismatch $\delta_{nl,1}^r$ equal to -10.82 ($\Lambda_{nl}^r = 3.53 \times 10^{-3}$), i.e. it corresponds roughly to the first local minimum of λ_{s_F} in the curve in Fig. 4a. We can clearly see that an efficient nonlinear interaction occurs in strips that correspond to transmission peaks; the larger the number m of a transmission peak [see Eq. (40)] the weaker the effective nonlinear interaction. The necessity to fulfill also the condition for perfect overall phase matching given in Eq. (35) is evident. The principal squeeze variance λ_{s_F} reaches values around 0.2 inside the strips around the first several transmission peaks. The larger the number m of a transmission peak, the greater values of linear coupling constant K_p^r and linear phase-mismatch δ_p^r have to be used to reach high levels of squeezing. Up to several forward-propagating photons can be present inside the waveguide (see Fig. 5b) at a given time instant. This means that the power of the outgoing field is of the order of 10^{-8} W (energy of one second-subharmonic photon inside the waveguide of thickness $t = 5 \times 10^{-7}$ m and length $L = 1 \times 10^{-3}$ m corresponds to the output power of 2.58×10^{-8} W). Only the first and the second transmission peaks can give reasonable values of the power of the outgoing field.

Role of the value of nonlinear phase mismatch $\delta_{nl,1}^r$ to squeezed-light generation is revealed in Fig. 6, where the principal squeeze variance λ_{s_F} as a function of the non-

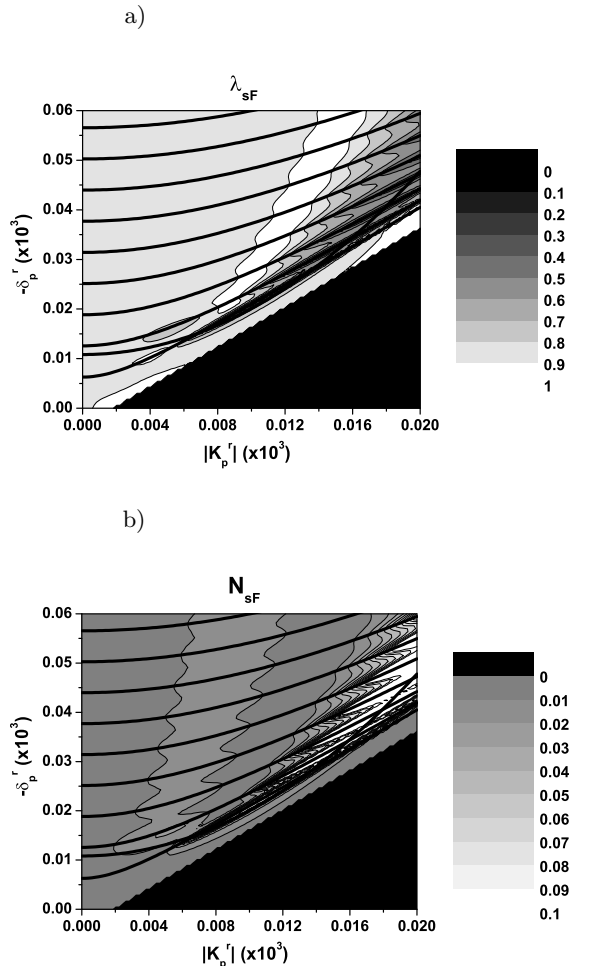


FIG. 5: Contour plots of principal squeeze variance λ_{sF} (a) and number N_{sF} of photons leaving the waveguide (b) for the forward-propagating second-subharmonic field as they depend on parameters $|K_p^r|$ and δ_p^r of the corrugation in the pump field; more-less equidistant curves in the graphs indicate positions of transmission peaks [Eq. (40)], the last curve going up gives the condition in Eq. (35); $\Lambda_{nl}^r = 3.53 \times 10^{-3}$ ($\delta_{nl,1}^r = -10.82$), $P_{pF} = 2$ W, $P_{sF} = 1 \times 10^{-10}$ W, $\arg(K_p^r) = \pi/2$; values of the other parameters are the same as in Fig. 4. Triangles in lower right corners with formally zero values in both graphs lie in the region with an exponential behavior of classical amplitudes that is not suitable for nonclassical-light generation.

linear phase mismatch $\delta_{nl,1}^r$ under the conditions given in Eqs. (41) and (43) is drawn for the first two transmission peaks ($m = 1, 2$). The larger the value of $\delta_{nl,1}^r$ the better the values of the principal squeeze variance λ_{sF} , but also the greater the values of linear coupling constant $|K_p^r|$ and linear phase mismatch δ_p^r (as shown in Figs 6b and 6c). The smallest values of $|K_p^r|$ and δ_p^r are obtained when the generation occurs around the first transmission peak. From practical point of view, the depth of linear corrugation is limited by technological reasons (also validity of

the model has to be judged for greater values of the linear coupling constant K_p^r) and this means that only smaller values of the linear coupling constant K_p are available (see Fig. 3). In order to obtain the best possible value of the principal squeeze variance λ_{sF} the curves in Fig. 6 suggest to work in the first transmission peak and use the greatest available value of K_p^r (the deepest possible corrugation). From the curve in Fig. 6b the appropriate value of the nonlinear phase mismatch $\delta_{nl,1}^r$ is determined and then the curve in Fig. 6c gives a suitable value of the linear phase mismatch δ_p^r (and consequently the period Λ_l of linear corrugation). Keeping the incident pump-field power fixed, the depth t_l of the corrugation limits the achievable values of the principal squeeze variance λ_{sF} ; the deeper the corrugation, the better the squeezing. We can roughly say that the appropriate values of linear coupling constant K_p^r and linear phase mismatch δ_p^r are close (or higher) to the value of nonlinear phase mismatch $\delta_{nl,1}^r$ to have an optimum phase matching (see Figs. 6b,c).

The curves in Fig. 6a also reveal the role of length L of the waveguide in squeezed-light generation. Because the nonlinear phase mismatch $\delta_{nl,1}$ does not depend on the length L , the dimensionless nonlinear phase mismatch $\delta_{nl,1}^r$ depicted in Fig. 6a is linearly proportional to the length L and so the larger the value of length L the lower the value of the principal squeeze variance λ_{sF} . The analysis of expressions in Eqs. (41) and (43) shows that in the limit of large length L , $|K_p| \rightarrow \delta_{nl,1}$ and $\delta_p \rightarrow 2\delta_{nl,1}$. We note that the distance of the adjacent transmission peaks in the plane spanned by variables $|K_p|$ and δ_p behaves as $1/L$ (see, e.g., graphs in Fig. 5).

In case of the considered LiNbO₃ waveguide, values of the natural nonlinear phase mismatch $\delta_{nl,0}$ for the considered values of thickness t as given in Fig. 2a are so high that in order to take advantage of scattering on the corrugation, an additional periodical poling has to be introduced to partially compensate for this mismatch [25].

Usefulness of the corrugation can be demonstrated when we compare the following three configurations: perfectly quasi-phase matched waveguide, non-perfectly quasi-phase matched waveguide, and finally non-perfectly quasi-phase matched waveguide with a suitable corrugation that compensates for phase mismatch. The waveguide with a corrugation gives better values of the principal squeeze variance λ_{sF} and also considerably greater values of the number N_{sF} of photons leaving the waveguide in the comparison with the perfectly quasi-phase-matched waveguide, as documented in Fig. 7. Also an improvement caused by an introduction of the corrugation into a non-perfectly quasi-phase-matched waveguide is worth mentioning.

A linear corrugation can be alternatively introduced into the second-subharmonic field. Despite the fact that the second-subharmonic field remains at single photon level, results obtained for principal squeeze variances λ and numbers N of photons are comparable to those achieved with a corrugation in the pump field. Suitable

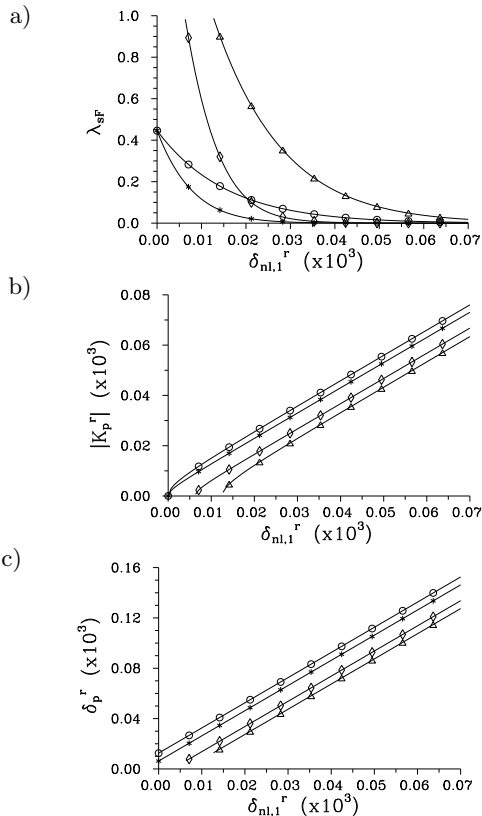


FIG. 6: Principal squeeze variance λ_{sF} (a), absolute value of the linear coupling constant K_p^r given by Eq. (43) (b), and linear phase mismatch δ_p^r determined along Eq. (41) (c) as functions of the nonlinear phase mismatch $\delta_{nl,1}^r$; first ($m=1$) and second ($m=2$) transmission peaks as well as signs $+$ and $-$ in Eq. (43) are considered ($m = 1+$: solid curve with $*$, $m = 1-$: solid curve with \diamond , $m = 2+$: solid curve with \circ , $m = 2-$: solid curve with \triangle); $P_{pF} = 2$ W, $P_{sF} = 1 \times 10^{-10}$ W, $\arg(K_p^r) = \pi/2$; values of the other parameters are the same as in Fig. 4.

conditions are given in Eqs. (38) and (40) in this case.

C. Second-harmonic generation

Second-harmonic generation requires a strong incident second-subharmonic field. As a reference we consider an incident power P_{sF} of the second-subharmonic field to be 2 W and periodical poling. We have for the principal squeeze variances $\lambda_{sF} \approx 0.87$ and $\lambda_{pF} \approx 0.99$ for the period of poling $\Lambda_{nl}^r \approx 3.552 \times 10^{-3}$ that assures a perfect quasi-phase matching (see Fig. 4b).

The nonlinearly interacting fields behave similarly as in the case of second-subharmonic generation. If we introduce a linear corrugation into the second-subharmonic field and set the nonlinear phase mismatch $\delta_{nl,1}^r$ equal to 3.53×10^{-3} (see Fig. 4b), values of the principal squeeze variance λ_{sF} approach 0.6 inside the strips in the plane spanned by variables $|K_s^r|$ and δ_s^r where the conditions

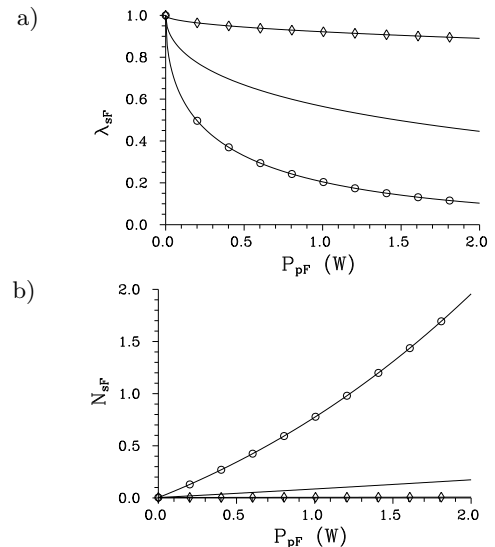


FIG. 7: Principal squeeze variance λ_{sF} (a) and number N_{sF} of photons leaving the waveguide for the forward-propagating second-subharmonic field as they depend on the incident pump-field power P_{pF} under different conditions: perfect quasi-phase matching ($\delta_{nl,1}^r = 0$) without a corrugation (solid curve), quasi-phase matching with $\Lambda_{nl}^r = 3.53 \times 10^{-3}$ ($\delta_{nl,1}^r = -10.82$) without a corrugation (solid curve with \diamond), and quasi-phase matching with $\Lambda_{nl}^r = 3.53 \times 10^{-3}$ together with a corrugation [its parameters are given by the conditions in Eqs. (43) ($m = 1$) and (35)] (solid curve with \circ); $P_{pF} = 2$ W, $P_{sF} = 1 \times 10^{-10}$ W, $\arg(K_p^r) = \pi/2$; values of the other parameters are the same as in Fig. 4.

from Eqs. (38) and (40) are fulfilled. The number N_{sF} of second-subharmonic photons at the output of the waveguide (together with the output power) decreases by an order of magnitude inside these strips compared to the incident power as a consequence of transfer of energy from the strong second-subharmonic field into the pump field (due to an efficient nonlinear interaction) and also transfer of energy into the backward-propagating field (due to scattering) is considerable. Despite this the squeezed second-subharmonic field remains very strong, it contains about 10^6 photons inside the waveguide. An appropriate choice of the value of nonlinear phase mismatch $\delta_{nl,1}^r$ is governed by the same rules as mentioned for second-subharmonic generation. The pump field that is only weakly squeezed for perfect quasi-phase matching can reach values of the principal squeeze variance λ_{pF} around 0.8 assuming corrugation with parameters given by Eqs. (38) and (40). The pump field gets a considerable amount of energy from the second-subharmonic field and so typical values of the number N_{pF} of pump photons leaving the waveguide can reach 10^6 ; i.e. the output power is of the order of 10^{-1} W (energy of one pump photon inside the waveguide of thickness $t = 5 \times 10^{-7}$ m and length $L = 1 \times 10^{-3}$ m corresponds to the output power of 5.13×10^{-8} W). A detailed behavior of the pump field with respect to the parameters of the linear corrugation

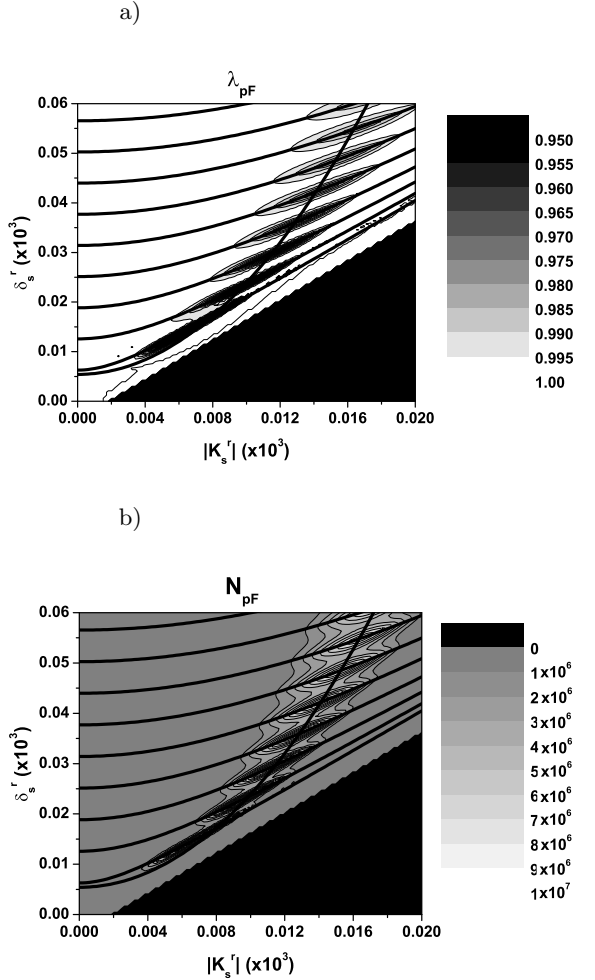


FIG. 8: Contour plots of principal squeeze variance λ_{pF} (a) and number N_{pF} of photons leaving the waveguide (b) for the forward-propagating pump field as they depend on parameters $|K_s^r|$ and δ_s^r of the linear corrugation in the second-subharmonic field; more-less equidistant curves in graphs indicate positions of transmission peaks [Eq. (40)], the last curve going up is given by Eq. (38); $\Lambda_{nl}^r = 3.53 \times 10^{-3}$ ($\delta_{nl,1}^r = -10.82$), $P_{pF} = 1 \times 10^{-10}$ W, $P_{sF} = 2$ W, $\arg(K_s^r) = \pi/2$; values of the other parameters are the same as in Fig. 4. As for triangles in lower right corners of both graphs with formally zero values, see caption to Fig. 5.

can be understood from graphs in Fig. 8.

A linear corrugation can also be put into the pump field and we arrive at qualitatively the same results as if the corrugation is present in the second-subharmonic field. For the value of nonlinear phase mismatch $\delta_{nl,1}^r = -10.82$ used above, values of the principal squeeze variance λ_{sF} can reach even 0.3. On the other hand, values of the principal squeeze variance λ_{pF} lie above 0.9.

At the end of discussion we make a note about the influence of some phases with respect to squeezed-light generation. It can be easily shown that any solution of

Eqs. (8) depends only on phase $\psi = \arg(K_p) - 2\arg(K_s)$. In our numerical investigations, we did not observe any dependence of numbers N of photons as well as principle squeeze variances λ on the phase ψ . On the other hand, these quantities depend weakly on phases $\arg(A_{sF})$ and $\arg(A_{pF})$ of the incident fields. However, this dependence is very weak under the conditions where a strongly squeezed light is generated.

V. MODEL FOR A MULTI-MODE NONLINEAR INTERACTION

We generalize the model presented for cw pumping in Sec. II to multi-mode fields using quantum theory. Because of the necessity to include also inter-mode dispersion, we decompose the electric-field operator amplitudes $\hat{\mathbf{E}}_a$ ($a = p, s$) using mode operator amplitudes \hat{a}_a in the Heisenberg picture [5, 8]:

$$\hat{\mathbf{E}}_a(x, y, z, t) = \int_0^\infty d\omega_a \hat{\mathbf{E}}_a(x, y, z, \omega_a) \exp(-i\omega_a t), \quad (48)$$

$$\hat{\mathbf{E}}_a(x, y, z, \omega_a) = i [\hat{a}_{aF}(z, \omega_a) \mathbf{e}_a(x, y, \omega_a) + \hat{a}_{aB}(z, \omega_a) \mathbf{e}_a(x, y, \omega_a) - \text{H.c.}], \quad a = p, s, \quad (49)$$

where $\hat{a}_{aF}(z, \omega_a)$ [$\hat{a}_{aB}(z, \omega_a)$] denotes annihilation operator of mode with frequency ω_a in field a propagating forward [backward]. We note that mode functions \mathbf{e}_a derived in Appendix A as well as propagation constants β_a depend on the frequency ω_a in the multi-mode model.

Evolution of quantum optical fields inside the studied waveguide is described using the following momentum operator \hat{G} [8, 20]:

$$\begin{aligned} \hat{G}(z) = & \sum_{a=p,s} \sum_{b=F,B} \int_0^\infty d\omega_a \hbar \beta_{ab}(\omega_a) \hat{a}_{ab}^\dagger(z, \omega_a) \hat{a}_{ab}(z, \omega_a) \\ & + \left[\sum_{a=p,s} \int_0^\infty d\omega_a \hbar K_a(\omega_a) \hat{a}_{aF}^\dagger(z, \omega_a) \hat{a}_{aB}(z, \omega_a) + \text{H.c.} \right] \\ & - \left[\sum_{b=F,B} 2i \int_0^\infty d\omega_s \int_0^\infty d\omega'_s K_{nl,q}(\omega_s, \omega'_s) \right. \\ & \times \hat{a}_{sb}^\dagger(z, \omega_s) \hat{a}_{sb}^\dagger(z, \omega'_s) \hat{a}_{pb}(z, \omega_s + \omega'_s) + \text{H.c.} \left. \right]. \quad (50) \end{aligned}$$

The Heisenberg equations written in Eq. (13) and corresponding to the momentum operator \hat{G} in Eq. (50) take the form:

$$\begin{aligned} \frac{d\hat{a}_{sF}(z, \omega_s)}{dz} = & i\beta_s(\omega_s) \hat{a}_{sF}(z, \omega_s) + iK_s(\omega_s) \hat{a}_{sB}(z, \omega_s) \\ & + 4 \int_0^\infty d\omega'_s K_{nl,q}(\omega_s, \omega'_s) \hat{a}_{pF}(z, \omega_s + \omega'_s) \hat{a}_{sF}^\dagger(z, \omega'_s), \\ \frac{d\hat{a}_{sB}(z, \omega_s)}{dz} = & -i\beta_s(\omega_s) \hat{a}_{sB}(z, \omega_s) - iK_s^*(\omega_s) \hat{a}_{sF}(z, \omega_s) \\ & - 4 \int_0^\infty d\omega'_s K_{nl,q}(\omega_s, \omega'_s) \hat{a}_{pB}(z, \omega_s + \omega'_s) \hat{a}_{sB}^\dagger(z, \omega'_s), \end{aligned}$$

$$\begin{aligned}
\frac{d\hat{a}_{p_F}(z, \omega_p)}{dz} &= i\beta_p(\omega_p)\hat{a}_{p_F}(z, \omega_p) + iK_p(\omega_p)\hat{a}_{p_B}(z, \omega_p) \\
&- 2 \int_0^\infty d\omega_s K_{nl,q}^*(\omega_s, \omega_p - \omega_s)\hat{a}_{s_F}(z, \omega_s)\hat{a}_{s_F}(z, \omega_p - \omega_s), \\
\frac{d\hat{a}_{p_B}(z, \omega_p)}{dz} &= -i\beta_p(\omega_p)\hat{a}_{p_B}(z, \omega_p) - iK_p^*(\omega_p)\hat{a}_{p_F}(z, \omega_p) \\
&+ 2 \int_0^\infty d\omega_s K_{nl,q}^*(\omega_s, \omega_p - \omega_s)\hat{a}_{s_B}(z, \omega_s)\hat{a}_{s_B}(z, \omega_p - \omega_s).
\end{aligned} \tag{51}$$

Linear coupling constants K_s , K_p and nonlinear coupling constants $K_{nl,q}$ ($q = 0, \pm 1$) are given in Eqs. (11) and (12) and are frequency dependent. We note that the nonlinear coupling constants $K_{nl,q}$ have the following symmetry: $K_{nl,q}(\omega_s, \omega'_s) = K_{nl,q}(\omega'_s, \omega_s)$.

Creation and annihilation operator amplitudes of the incident fields are assumed to fulfill boson commutation relations, i.e.

$$\begin{aligned}
[\hat{a}_{a_F}(0, \omega_a), \hat{a}_{a'_F}^\dagger(0, \omega_{a'})] &= \delta_{a,a'}\delta(\omega_a - \omega_{a'}), \\
[\hat{a}_{a_B}(L, \omega_a), \hat{a}_{a'_B}^\dagger(L, \omega_{a'})] &= \delta_{a,a'}\delta(\omega_a - \omega_{a'}), \\
a &= p, s
\end{aligned} \tag{52}$$

and the remaining commutators are zero. It can be shown [49] for quadratic momentum operators \hat{G} that also the output operator amplitudes have to obey boson commutation relations:

$$\begin{aligned}
[\hat{a}_{a_F}(L, \omega_a), \hat{a}_{a'_F}^\dagger(L, \omega_{a'})] &= \delta_{a,a'}\delta(\omega_a - \omega_{a'}), \\
[\hat{a}_{a_B}(0, \omega_a), \hat{a}_{a'_B}^\dagger(0, \omega_{a'})] &= \delta_{a,a'}\delta(\omega_a - \omega_{a'}), \\
a &= p, s
\end{aligned} \tag{53}$$

and commutators not mentioned in Eqs. (53) are zero.

The nonlinear operator equations written in Eqs. (51) have one integral of motion that expresses the conservation law of the overall energy:

$$\begin{aligned}
\frac{d}{dz} \left[\int_0^\infty d\omega_s \hat{a}_{s_F}^\dagger(z, \omega_s)\hat{a}_{s_F}(z, \omega_s) \right. \\
- \int_0^\infty d\omega_s \hat{a}_{s_B}^\dagger(z, \omega_s)\hat{a}_{s_B}(z, \omega_s) \\
+ 2 \int_0^\infty d\omega_p \hat{a}_{p_F}^\dagger(z, \omega_p)\hat{a}_{p_F}(z, \omega_p) \\
\left. - 2 \int_0^\infty d\omega_p \hat{a}_{p_B}^\dagger(z, \omega_p)\hat{a}_{p_B}(z, \omega_p) \right] = 0.
\end{aligned} \tag{54}$$

When solving evolution of the nonlinearly interacting fields as described in Eqs. (51) electric-field operator amplitudes \hat{A}_{s_F} , \hat{A}_{s_B} , \hat{A}_{p_F} , and \hat{A}_{p_B} in the interaction representation can be conveniently defined ($\hat{a}_{a_F}(z, \omega_a) = \hat{A}_{a_F}(z, \omega_a)\exp[i\beta_a(\omega_a)z]$, $\hat{a}_{a_B}(z, \omega_a) = \hat{A}_{a_B}(z, \omega_a)\exp[-i\beta_a(\omega_a)z]$, $a = p, s$) transforming the equations in Eqs. (51) into the form:

$$\frac{d\hat{A}_{s_F}(z, \omega_s)}{dz} = iK_s(\omega_s)\exp[-i\delta_s(\omega_s)z]\hat{A}_{s_B}(z, \omega_s)$$

$$\begin{aligned}
&+ 4 \int_0^\infty d\omega'_s K_{nl,q}(\omega_s, \omega'_s)\exp[i\delta_{nl,q}(\omega_s, \omega'_s)z] \\
&\times \hat{A}_{p_F}(z, \omega_s + \omega'_s)\hat{A}_{s_F}^\dagger(z, \omega'_s), \\
\frac{d\hat{A}_{s_B}(z, \omega_s)}{dz} &= -iK_s^*(\omega_s)\exp[i\delta_s(\omega_s)z]\hat{A}_{s_F}(z, \omega_s) \\
&- 4 \int_0^\infty d\omega'_s K_{nl,q}(\omega_s, \omega'_s)\exp[-i\delta_{nl,q}(\omega_s, \omega'_s)z] \\
&\times \hat{A}_{p_B}(z, \omega_s + \omega'_s)\hat{A}_{s_B}^\dagger(z, \omega'_s), \\
\frac{d\hat{A}_{p_F}(z, \omega_p)}{dz} &= iK_p(\omega_p)\exp[-i\delta_p(\omega_p)z]\hat{A}_{p_B}(z, \omega_p) \\
&- 2 \int_0^\infty d\omega_s K_{nl,q}^*(\omega_s, \omega_p - \omega_s)\exp[-i\delta_{nl,q}(\omega_s, \omega_p - \omega_s)z] \\
&\times \hat{A}_{s_F}(z, \omega_s)\hat{A}_{s_F}(z, \omega_p - \omega_s), \\
\frac{d\hat{A}_{p_B}(z, \omega_p)}{dz} &= -iK_p^*(\omega_p)\exp[i\delta_p(\omega_p)z]\hat{A}_{p_F}(z, \omega_p) \\
&+ 2 \int_0^\infty d\omega_s K_{nl,q}^*(\omega_s, \omega_p - \omega_s)\exp[i\delta_{nl,q}(\omega_s, \omega_p - \omega_s)z] \\
&\times \hat{A}_{s_B}(z, \omega_s)\hat{A}_{s_B}(z, \omega_p - \omega_s).
\end{aligned} \tag{55}$$

Linear phase mismatches δ_p , δ_s and nonlinear phase mismatches $\delta_{nl,q}$ ($q = 0, \pm 1$) are defined as follows:

$$\begin{aligned}
\delta_a(\omega_a) &= 2\beta_a(\omega_a) - \frac{2\pi}{\Lambda_l}, \quad a = p, s, \\
\delta_{nl,q}(\omega_s, \omega'_s) &= \beta_p(\omega_s + \omega'_s) - \beta_s(\omega_s) - \beta_s(\omega'_s) + q\frac{2\pi}{\Lambda_{nl}}.
\end{aligned} \tag{56}$$

It holds that $\delta_{nl,q}(\omega_s, \omega'_s) = \delta_{nl,q}(\omega'_s, \omega_s)$.

VI. SECOND-SUBHARMONIC GENERATION WITH A LINEAR CORRUGATION IN A STRONG PUMP FIELD - PERTURBATION APPROACH

A strong incident pump field being scattered on a linear corrugation is considered. We also assume that the process of second-subharmonic generation is weak and the generated second-subharmonic field remains at single photon level. Because the generated second-subharmonic field is many orders of magnitude weaker than the pump field, depletion as well as quantum features of the pump field can be neglected and the last two equations in Eqs. (51) can be transformed into the equations for strong amplitudes a_{p_F} and a_{p_B} :

$$\begin{aligned}
\frac{da_{p_F}(z, \omega_p)}{dz} &= i\beta_p(\omega_p)a_{p_F}(z, \omega_p) + iK_p(\omega_p)a_{p_B}(z, \omega_p), \\
\frac{da_{p_B}(z, \omega_p)}{dz} &= -i\beta_p(\omega_p)a_{p_B}(z, \omega_p) - iK_p^*(\omega_p)a_{p_F}(z, \omega_p).
\end{aligned} \tag{57}$$

Solution for the forward-propagating pump-field amplitude a_{p_F} can be found in the form:

$$a_{p_F}(z, \omega_p) = \exp[i\beta_p(\omega_p)z]\exp(-i\delta_p z/2)$$

$$\times [\exp(i\Delta_p z)\mathcal{B}_{p_F}^+(\omega_p) + \exp(-i\Delta_p z)\mathcal{B}_{p_F}^-(\omega_p)], \quad (58)$$

where functions $\mathcal{B}_{p_F}^\pm$ ($\mathcal{B}_{p_F}^- = \mathcal{B}_{p_F}^{+*}$) are given by boundary conditions, i.e. by spectrum of the incident pump pulse. If the central frequency ω_p^0 is tuned at a transmission peak [$\Delta_p^0 L = m\pi$, $m = 1, 2, \dots$, $\delta_p^0 = \delta_p(\omega_p^0)$] we may approximately write:

$$\begin{aligned} a_{p_F}(z, \omega_p) &= \exp[i\beta_p(\omega_p)z] \exp(-i\delta_p^0 z/2) \\ &\times [\exp(i\Delta_p^0 z)\mathcal{B}_{p_F}^{0+}(\omega_p) + \exp(-i\Delta_p^0 z)\mathcal{B}_{p_F}^{0-}(\omega_p)], \\ \mathcal{B}_{p_F}^{0+}(\omega_p) &= \frac{2\Delta_p^0 + \delta_p^0}{4\Delta_p^0} A_{p_F}(0, \omega_p); \end{aligned} \quad (59)$$

$A_{p_F}(0, \omega_p)$ means the incident pump-field amplitude spectrum.

An operator perturbation solution of the first equation in Eqs. (51) with the substituted pump-field amplitude a_{p_F} as written in Eq. (59) is obtained in the form:

$$\begin{aligned} \hat{a}_{s_F}(L, \omega_s) &= \int_0^\infty d\omega'_s U(\omega_s, \omega'_s) \hat{a}_{s_F}(0, \omega'_s) \\ &+ \int_0^\infty d\omega'_s V(\omega_s, \omega'_s) \hat{a}_{s_F}^\dagger(0, \omega'_s), \end{aligned} \quad (60)$$

$$U(\omega_s, \omega'_s) = \delta(\omega_s - \omega'_s) \exp[i\beta_s(\omega_s)L], \quad (61)$$

$$\begin{aligned} V(\omega_s, \omega'_s) &= -i4K_{nl,q}(\omega_s, \omega'_s) \exp[i\beta_s(\omega_s)L] \\ &\times \exp\left(i\left[\delta_{nl,q}(\omega_s, \omega'_s) - \frac{\delta_p^0}{2} \pm \Delta_p^0\right] \frac{L}{2}\right) \\ &\times \frac{L}{2} \text{sinc}\left(\left[\delta_{nl,q}(\omega_s, \omega'_s) - \frac{\delta_p^0}{2} \pm \Delta_p^0\right] \frac{L}{2}\right) \\ &\times \mathcal{B}_{p_F}^{0\pm}(\omega_s + \omega'_s); \end{aligned} \quad (62)$$

$\text{sinc}(x) = \sin(x)/x$. Two different solutions are written in Eqs. (60–62): one solution is appropriate under the condition $\delta_{nl,q}(\omega_s, \omega'_s) - \delta_p^0/2 + \Delta_p^0 \approx 0$ whereas the second one is valid when $\delta_{nl,q}(\omega_s, \omega'_s) - \delta_p^0/2 - \Delta_p^0 \approx 0$. We note that one of these two conditions has to be fulfilled in order to observe an efficient second-subharmonic generation as has been shown for cw case in Sec. III.

In our first-order perturbation approach, the Green function U as given in Eq. (61) describes free-field evolution whereas the Green function V in Eq. (62) characterizes properties of a generated photon pair. The Green function V is closely related to the so-called two-photon amplitude Φ introduced in the description of spontaneous parametric down-conversion [50–52]. Similarly as a two-photon amplitude Φ the Green function V can be decomposed into the Schmidt decomposition that gives typical eigenmodes of the nonlinear interaction. This decomposition can be reached even analytically under the following conditions. We first assume that the nonlinear coupling constant $K_{nl,q}$ does not depend on frequencies and express the propagation constants β_a in Taylor series:

$$\beta_a(\omega_a) = \beta_a^0 + \beta_{1,a}(\omega_a - \omega_a^0) + \beta_{2,a}(\omega_a - \omega_a^0)^2/2;$$

$$\begin{aligned} \beta_a^0 &= \beta_a(\omega_a^0), \\ \beta_{i,a} &= \left. \frac{d^i \beta_a}{d\omega_a^i} \right|_{\omega_a=\omega_a^0}, \quad i = 1, 2; \quad a = p, s. \end{aligned} \quad (63)$$

The sinc function occurring in Eq. (62) can be approximated by a gaussian function along the relation:

$$\begin{aligned} \text{sinc}\left[\alpha_0 + \alpha_1(\omega_s + \omega'_s - \omega_p^0) + \alpha_2(\omega_s + \omega'_s - \omega_p^0)^2\right. \\ \left.+ \alpha_3(\omega_s - \omega'_s)^2\right] \approx \\ \exp\left[-\frac{|\alpha_3|}{3}(\omega_s - \omega'_s)^2 - \frac{\alpha_1^2}{5}\left(\omega_s + \omega'_s - \omega_p^0 + \frac{\alpha_0}{\alpha_1}\right)^2\right], \end{aligned} \quad (64)$$

where α_0 , α_1 , α_2 , and α_3 are constants and α_2 can be neglected for values of parameters typical for the considered waveguide. An incident gaussian pump pulse with such phase modulation along the spectrum that phases of different frequencies are equal in the middle of the waveguide is further assumed [34], i.e.

$$\begin{aligned} A_{p_F}(0, \omega_p) &= A_{p_F} \exp\left(\frac{-i[\beta_p(\omega_p) - \beta_p^0]L}{2}\right) \\ &\times \sqrt{\frac{\tau_p}{\sqrt{2\pi}^3}} \exp\left[-\frac{\tau_p^2(\omega_p - \omega_p^0)^2}{4}\right] \end{aligned} \quad (65)$$

and τ_p denotes pump-pulse duration. Constant A_{p_F} in Eq. (65) gives strength of the pump pulse and is determined from the incident pump power P_{p_F} along the formula in Eq. (45). We note that $\int_0^\infty d\omega_p |A_{p_F}(0, \omega_p)|^2 = |A_{p_F}|^2/2\pi$. The Green function V finally gets the gaussian form:

$$\begin{aligned} V(\omega_s, \omega'_s) &= -iK_{nl,q}^0 L \frac{2\Delta_p^0 + \delta_p^0}{2\Delta_p^0} \sqrt{\frac{\tau_p}{\sqrt{2\pi}^3}} \\ &\times \exp\left[i\left(\frac{2\pi q}{\Lambda_{nl}} - \frac{\delta_p^0}{2} \pm \Delta_p^0\right) \frac{L}{2}\right] \Phi(\omega_s, \omega'_s), \quad (66) \\ \Phi(\omega_s, \omega'_s) &= \exp\left(i\left[\beta_s(\omega_s) - \beta_s(\omega'_s)\right] \frac{L}{2}\right) \tilde{\Phi}(\omega_s, \omega'_s), \end{aligned} \quad (67)$$

$$\begin{aligned} \tilde{\Phi}(\omega_s, \omega'_s) &= \exp\left[-\frac{(\omega_s - \omega'_s)^2}{\Delta_-^2}\right] \\ &\times \exp\left(-\frac{[\omega_s + \omega'_s - \omega_p^0 + \delta_{nl,q}^0/(\beta_{1,p} - \beta_{1,s})]^2}{\Delta_+^2}\right); \end{aligned} \quad (68)$$

$K_{nl,q}^0 = K_{nl,q}(\omega_s^0, \omega_s^0)$. Parameters Δ_+ and Δ_- of the Green function V are given as:

$$\begin{aligned} \frac{1}{\Delta_-^2} &= \frac{\beta_{2,s}L}{24}, \\ \frac{1}{\Delta_+^2} &= \frac{(\beta_{1,p} - \beta_{1,s})^2 L^2}{20} + \frac{\tau_p^2}{4}. \end{aligned} \quad (69)$$

The gaussian function $\tilde{\Phi}$ given in Eq. (68) can be decomposed into the Schmidt decomposition [34, 54]:

$$\tilde{\Phi}(\omega_s, \omega'_s) = \sum_{n=0}^{\infty} \mu_n \tilde{\phi}_n(\omega_s) \tilde{\phi}_n(\omega'_s). \quad (70)$$

Eigenvalues μ_n are given as follows:

$$\mu_n = 2\sqrt{\frac{\pi}{\Delta_+ \Delta_-}} \theta^{n/2}, \quad (71)$$

$$\theta = \left(\frac{\Delta_+ - \Delta_-}{\Delta_+ + \Delta_-} \right)^2. \quad (72)$$

Eigenmode functions $\tilde{\phi}_n$ can be expressed in terms of the Hermite polynomials H_n :

$$\begin{aligned} \tilde{\phi}_n(\omega_s) &= \sqrt{\frac{\tau_s}{2^n n! \sqrt{\pi}}} \exp[-\tau_s^2 (\omega_s - \bar{\omega}_s)^2] \\ &\quad \times H_n(\tau_s [\omega_s - \bar{\omega}_s]), \end{aligned} \quad (73)$$

$$\begin{aligned} \tau_s &= \sqrt{\frac{1 - \theta^2}{\theta}}, \\ \bar{\omega}_s &= \frac{\omega_p^0}{2} - \frac{\delta_{nl,q}^0}{2(\beta_{1,p} - \beta_{1,s})}. \end{aligned} \quad (74)$$

For the considered waveguide, $\Delta_+ \ll \Delta_-$ and thus a typical time constant τ_s defined in Eqs. (74) can be approximated as:

$$\tau_s \approx 8 \frac{\Delta_+}{\Delta_-}. \quad (75)$$

Taking into account inter-mode phase modulation as it appears in Eq. (67) eigenmode functions ϕ_n of the nonlinear interaction are given as follows:

$$\phi(\omega_s) = \exp[i\beta_s(\omega_s)L/2] \tilde{\phi}(\omega_s) \quad (76)$$

and the function Φ written in Eq. (67) attains its Schmidt decomposition [34]:

$$\Phi(\omega_s, \omega'_s) = \sum_{n=0}^{\infty} \mu_n \phi_n(\omega_s) \phi_n^*(\omega'_s). \quad (77)$$

The Schmidt decomposition of function Φ written in Eq. (77) suggests to introduce new discrete sets of annihilation and creation operator amplitudes that diagonalize the nonlinear interaction:

$$\hat{a}_{sF,n}^{in} = \int_0^\infty d\omega_s \phi_n(\omega_s) \hat{a}_{sF}(0, \omega_s), \quad (78)$$

$$\hat{a}_{sF,n}^{out} = \int_0^\infty d\omega_s \phi_n^*(\omega_s) \hat{a}_{sF}(L, \omega_s). \quad (79)$$

Because functions ϕ_n (ϕ_n^*) form an orthonormal basis, operators $\hat{a}_{sF,n}^{in}$ and $\hat{a}_{sF,n}^{out\dagger}$ ($\hat{a}_{sF,n}^{out}$ and $\hat{a}_{sF,n}^{out\dagger}$) fulfill the usual boson commutation relations.

Enhancement of the nonlinear interaction caused by scattering of the pump field on a linear corrugation is

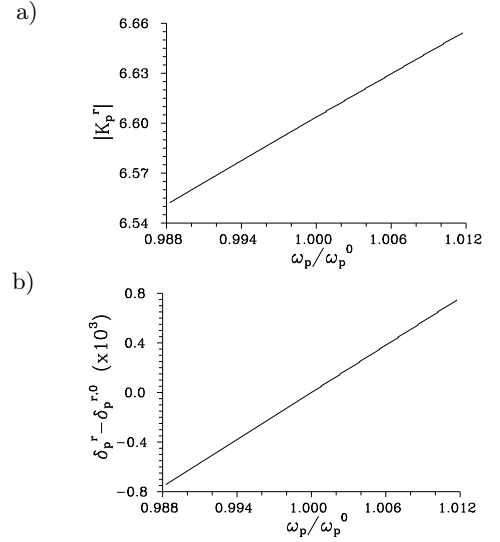


FIG. 9: Absolute value of the linear coupling constant K_p^r (a) and relative linear phase mismatch $\delta_p^r - \delta_p^{r,0}$ (b) for the pump field as they depend on the relative frequency ω_p/ω_p^0 , $\delta_p^{r,0} = L\delta_p(\omega_p^0)$; $t = 5 \times 10^{-7}$ m, $t_l = 5 \times 10^{-8}$ m.

contained in a multiplicative factor $(2\Delta_p^0 + \delta_p^0)/(4\Delta_p^0)$ in Eq. (66) that can be expressed as follows:

$$\mathcal{M} = \frac{2\Delta_p^0 + \delta_p^0}{4\Delta_p^0} = \frac{1}{2} + \frac{1}{2} \sqrt{\frac{|K_p^0|^2 + (m\pi/L)^2}{(m\pi/L)^2}}. \quad (80)$$

The greatest value of enhancement factor \mathcal{M} is reached at the first transmission peak ($m = 1$) and the greater the value of linear coupling constant K_p^0 the greater the value of enhancement factor \mathcal{M} . On the other hand there is no enhancement in the limit $m \rightarrow \infty$, i.e. the effect of pump-field localization is lost.

VII. SECOND-SUBHARMONIC GENERATION WITH A LINEAR CORRUGATION IN A STRONG PUMP FIELD - NON-PERTURBATION APPROACH

Linear coupling constants K_p , K_s and nonlinear coupling constants $K_{nl,q}$ depend only weakly on frequencies in a relatively broad range. This is documented in Figs. 9a, 10a, and 11a where the dimensionless constants [for their definitions, see Eqs. (47)] K_s^r , K_p^r , and $K_{nl,1}^r$, respectively, are plotted as functions of frequencies in the range of cca 20 nm for typical values of the waveguide parameters.

If inter-mode dispersion is omitted, equations for operator amplitudes $\hat{A}_{ab}(z, \omega)$ given in Eqs. (55) can be decoupled using Fourier transform:

$$\hat{A}_{ab}(z, \omega_a) = \frac{1}{2\pi} \int_{-\infty}^{\infty} d\tau_a \hat{A}_{ab}(z, \tau) \exp(i\omega_a \tau_a). \quad (81)$$

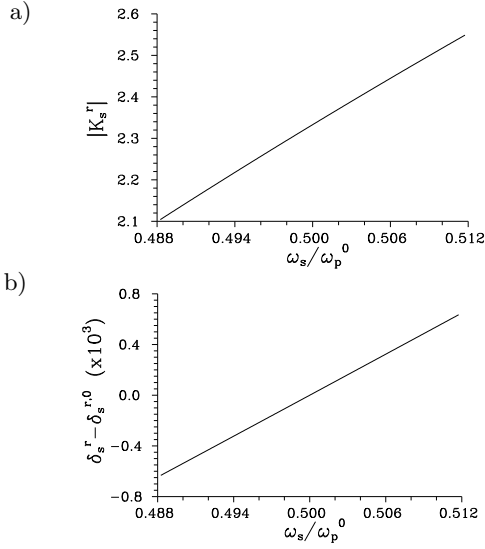


FIG. 10: Absolute value of the linear coupling constant K_s^r (a) and relative linear phase mismatch $\delta_s^r - \delta_s^{r,0}$ (b) for the second-subharmonic field as functions of the relative frequency ω_s/ω_p^0 , $\delta_s^{r,0} = L\delta_s(\omega_s^0)$; values of parameters are the same as in Fig. 9.

The system of equations in Eqs. (55) attains the following form after Fourier transform:

$$\begin{aligned}
 \frac{d\hat{A}_{sF}(z, \tau)}{dz} &= 4K_{nl,q}^0 \exp(i\delta_{nl,q}^0 z) \hat{A}_{pF}(z, \tau) \hat{A}_{sF}^\dagger(z, \tau), \\
 \frac{d\hat{A}_{sB}(z, \tau)}{dz} &= -4K_{nl,q}^0 \exp(-i\delta_{nl,q}^0 z) \hat{A}_{pB}(z, \tau) \hat{A}_{sB}^\dagger(z, \tau), \\
 \frac{d\hat{A}_{pF}(z, \tau)}{dz} &= iK_p^0 \exp(-i\delta_p^0 z) \hat{A}_{pB}(z, \tau) \\
 &\quad - 2K_{nl,q}^{0*} \exp(-i\delta_{nl,q}^0 z) \hat{A}_{sF}^2(z, \tau), \\
 \frac{d\hat{A}_{pB}(z, \tau)}{dz} &= -iK_p^{0*} \exp(i\delta_p^0 z) \hat{A}_{pF}(z, \tau) \\
 &\quad + 2K_{nl,q}^{0*} \exp(i\delta_{nl,q}^0 z) \hat{A}_{sB}^2(z, \tau); \quad (82)
 \end{aligned}$$

$K_a^0 = K_a(\omega_a^0)$, $\delta_a^0 = \delta_a(\omega_a^0)$ ($a = p, s$), $K_{nl,q}^0 = K_{nl,q}(\omega_s^0, \omega_p^0)$, and $\delta_{nl,q}^0 = \delta_{nl,q}(\omega_s^0, \omega_p^0)$. A suitable range of frequencies in which this approximation is valid can be guessed from the curves in Figs. 9b, 10b, and 11b showing the dependence of relative pump-field linear dephasing $\delta_p^r - \delta_p^{r,0}$, second-subharmonic linear dephasing $\delta_s^r - \delta_s^{r,0}$, and nonlinear dephasing $\delta_{nl,1}^r - \delta_{nl,1}^{r,0}$, respectively, on frequencies. The requirement to neglect inter-mode dispersion limits the length L of waveguide to smaller values.

If the incident pump field is strong, its depletion due to nonlinear interaction can be omitted. Solution of the last two equations in Eqs. (82) considered as equations for classical amplitudes A_{pF} and A_{pB} can then be found

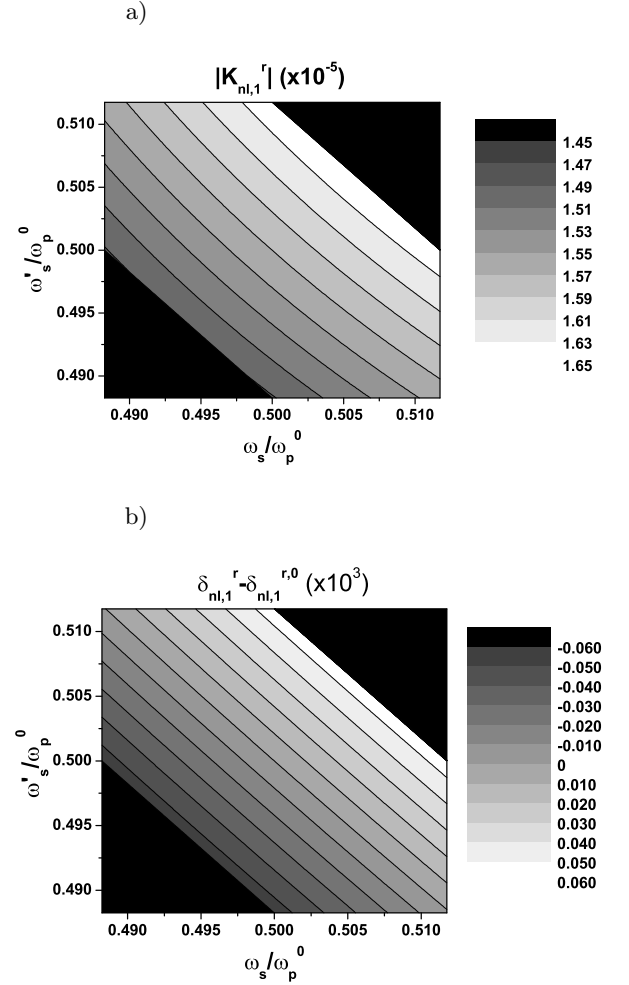


FIG. 11: Contour plots of the absolute value of nonlinear coupling constant $K_{nl,1}^r$ (a) and relative nonlinear phase mismatch $\delta_{nl,1}^r - \delta_{nl,1}^{r,0}$ (b) as they depend on relative frequencies ω_s/ω_p^0 and ω_s'/ω_p^0 . Values are shown only in the area $|\omega_s + \omega_s' - \omega_p^0| < \Delta\omega_p$, where $\Delta\omega_p$ gives a maximum allowed width of the pump-field spectrum, i.e. the black lower left and upper right triangles give no information. $\delta_{nl,1}^{r,0} = L\delta_{nl,1}(\omega_s^0, \omega_p^0)$; values of parameters are the same as in Fig. 9.

in a simple analytical form for transmission peaks:

$$\begin{aligned}
 A_{pF}(z, \tau_p) &= \exp(-i\delta_p^0 z/2) \\
 &\quad \times [\exp(i\Delta_p^0 z) \mathcal{B}_{pF}^{0+}(\tau_p) + \exp(-i\Delta_p^0 z) \mathcal{B}_{pF}^{0-}(\tau_p)], \\
 \mathcal{B}_{pF}^{0+}(\tau_p) &= \mathcal{M} A_{pF}(0, \tau_p). \quad (83)
 \end{aligned}$$

Symbol $A_{pF}(0, \tau_p)$ denotes the Fourier transform of incident pump-field amplitude spectrum $A_{pF}(0, \omega_p)$ and the enhancement factor \mathcal{M} is defined in Eq. (80).

The first operator equation in Eqs. (82) can be rewritten for two resonant conditions indicated in the expression for amplitude $A_{pF}(z, \tau)$ in Eq. (83) as follows:

$$\frac{d\hat{A}_{sF}(z, \tau)}{dz} = 4K_{nl,q}^0 \mathcal{B}_{pF}^{0\pm}(\tau)$$

$$\times \exp[i(\delta_{nl,q}^0 - \delta_p^0/2 \pm \Delta_p^0)z] \hat{A}_{s_F}^\dagger(z, \tau). \quad (84)$$

Substitution $\hat{A}_{s_F}(z, \tau) = \hat{\mathcal{A}}_{s_F}(z, \tau) \exp[i(\delta_{nl,q}^0/2 - \delta_p^0/4 \pm \Delta_p^0/2)z]$, $\hat{A}_{s_F}^\dagger(z, \tau) = \hat{\mathcal{A}}_{s_F}^\dagger(z, \tau) \exp[-i(\delta_{nl,q}^0/2 - \delta_p^0/4 \pm \Delta_p^0/2)z]$ in Eq. (84) leads to differential equations with constant coefficients for operator amplitudes $\hat{\mathcal{A}}_{s_F}$ and $\hat{\mathcal{A}}_{s_F}^\dagger$ that allow us to find solution of Eq. (84):

$$\hat{A}_{s_F}(L, \tau) = U(\tau) \hat{A}_{s_F}(0, \tau) + V(\tau) \hat{A}_{s_F}^\dagger(0, \tau), \quad (85)$$

$$U(\tau) = \frac{1}{2} \exp\left(i \frac{\Omega^\pm L}{2}\right) \times \left[\left(1 - \frac{i\Omega^\pm}{2\lambda^\pm(\tau)}\right) \exp[\lambda^\pm(\tau)L] + \left(1 + \frac{i\Omega^\pm}{2\lambda^\pm(\tau)}\right) \exp[-\lambda^\pm(\tau)L] \right], \quad (86)$$

$$V(\tau) = \frac{\mathcal{K}^\pm(\tau)}{2\lambda^\pm(\tau)} \exp\left(i \frac{\Omega^\pm L}{2}\right) \times [\exp[\lambda^\pm(\tau)L] - \exp[-\lambda^\pm(\tau)L]]. \quad (87)$$

Phase mismatches Ω^\pm , nonlinear coupling constants \mathcal{K}^\pm , and eigenvalues λ^\pm are given by the following formulas:

$$\begin{aligned} \Omega^\pm &= \delta_{nl,q}^0 - \delta_p^0/2 \pm \Delta_p^0, \\ \mathcal{K}^\pm(\tau) &= K_{nl,q}^0 \frac{2\Delta_p^0 + \delta_p^0}{\Delta_p^0} A_{p_F}(0, \tau), \\ \lambda^\pm(\tau) &= \sqrt{|\mathcal{K}^\pm(\tau)|^2 - \Omega^{\pm 2}/4}. \end{aligned} \quad (88)$$

Inverse Fourier transform of the expression for operator amplitude $\hat{A}_{s_F}(L, \tau)$ in Eq. (85) provides the operator amplitude $\hat{A}_{s_F}(L, \omega_s)$ and, after returning from the interaction representation, the following expression for the output second-subharmonic operator amplitude $\hat{a}_{s_F}(L, \omega_s)$ is reached:

$$\begin{aligned} \hat{a}_{s_F}(L, \omega_s) &= \exp[i\beta(\omega_s)L] \\ &\times \left[\int_0^\infty d\omega'_s U(\omega_s - \omega'_s) \hat{A}_{s_F}(0, \omega'_s) + \int_0^\infty d\omega'_s V(\omega_s + \omega'_s) \hat{A}_{s_F}^\dagger(0, \omega'_s) \right]. \end{aligned} \quad (89)$$

Functions $U(\omega)$ and $V(\omega)$ are given by inverse Fourier transform of the expressions occurring in Eqs. (86) and (87) and can be found numerically.

The general expression for continuous output operator amplitudes $\hat{a}_{s_F}(L, \omega_s)$ as it occurs in Eq. (60) has to be discretized in order to investigate the model numerically. We introduce discrete mode operator amplitudes $\hat{a}_{s_F,i}$ that are distant by $\Delta\omega$, i.e.

$$\hat{a}_{s_F,i}(z) = \sqrt{\Delta\omega} \hat{a}_{s_F}(z, \omega_s^0 + i\Delta\omega). \quad (90)$$

The Green functions U and V are then transformed into matrices \mathbf{U} and \mathbf{V} :

$$\begin{aligned} \mathbf{U}_{ij} &= \Delta\omega U(\omega_s^0 + i\Delta\omega, \omega_s^0 + j\Delta\omega), \\ \mathbf{V}_{ij} &= \Delta\omega V(\omega_s^0 + i\Delta\omega, \omega_s^0 + j\Delta\omega). \end{aligned} \quad (91)$$

Operator amplitudes $\hat{a}_{s_F,i}$ defined in Eq. (90) obey the usual boson commutation relations instead of those written in Eq. (53). Transformation written in Eq. (60) between the input second-subharmonic operator amplitudes $\hat{a}_{s_F,i}^{in}$, $\hat{a}_{s_F,i}^{in\dagger}$ and output second-subharmonic operator amplitudes $\hat{a}_{s_F,i}^{out}$, $\hat{a}_{s_F,i}^{out\dagger}$ can, after discretization, be written in the matrix form:

$$\hat{\mathbf{a}}_{s_F}^{out} = \mathbf{U} \hat{\mathbf{a}}_{s_F}^{in} + \mathbf{V} \hat{\mathbf{a}}_{s_F}^{in\dagger}. \quad (92)$$

Vectors $\hat{\mathbf{a}}_{s_F}^{in}$ and $\hat{\mathbf{a}}_{s_F}^{out}$ are composed of operator amplitudes $\hat{a}_{s_F,i}^{in}$ and $\hat{a}_{s_F,i}^{out}$, respectively.

Because the input operator amplitudes $\hat{a}_{s_F,i}^{in}$, $\hat{a}_{s_F,i}^{in\dagger}$ as well as the output operator amplitudes $\hat{a}_{s_F,i}^{out}$, $\hat{a}_{s_F,i}^{out\dagger}$ fulfill boson commutation relations the transformation written in Eq. (92) represents the Bogoljubov transformation. This means that matrices \mathbf{U} and \mathbf{V} can be decomposed using the Bloch—Messiah reduction [33, 34]:

$$\begin{aligned} \mathbf{U} &= \mathbf{X} \mathbf{\Lambda}_U \mathbf{Y}^\dagger, \\ \mathbf{V} &= \mathbf{X} \mathbf{\Lambda}_V \mathbf{Y}^T, \end{aligned} \quad (93)$$

where \dagger means hermitian conjugated matrix and T stands for matrix transposition. Matrices $\mathbf{\Lambda}_U$ and $\mathbf{\Lambda}_V$ are diagonal and contain nonnegative eigenvalues of the decomposition. Matrix \mathbf{Y} (\mathbf{X}) in Eq. (93) contains the right (left) eigenvectors.

Eigenvectors defined by the Bloch-Messiah reduction give typical modes of the nonlinear interaction and represent a discrete form of eigenmode functions ϕ_n found in Eq. (76) in analytical approach of Sec. VI.

Coefficients B_n and C_n of the generalized superposition of signal and noise [8] valid for the n th eigenmode and defined in Eqs. (24) can be expressed in terms of eigenvalues of the decomposition (an incident second-subharmonic field in vacuum state is assumed):

$$\begin{aligned} B_n &= (\mathbf{\Lambda}_V)_{nn}^2, \\ C_n &= (\mathbf{\Lambda}_U)_{nn} (\mathbf{\Lambda}_V)_{nn}. \end{aligned} \quad (94)$$

The second-subharmonic principal squeeze variance $\lambda_{s_F,n}$ of eigenmode n is then determined along the expression:

$$\lambda_{s_F,n} = 1 + 2(\mathbf{\Lambda}_V)_{nn} [(\mathbf{\Lambda}_V)_{nn} - (\mathbf{\Lambda}_U)_{nn}]. \quad (95)$$

The number $N_{s_F,n}$ of photons leaving the waveguide in eigenmode n is given by a simple formula ($N_{s_F} = \langle \hat{A}_{s_F}^\dagger \hat{A}_{s_F} \rangle$, averaging is over an incident second-subharmonic vacuum state):

$$N_{s_F,n} = (\mathbf{\Lambda}_V)_{nn}^2. \quad (96)$$

Importance of the Bloch-Messiah reduction in investigations of squeezing is emphasized by the fact that an eigenmode with the lowest value of the principal squeeze variance $\lambda_{s_F,i}$ represents the solution of the optimization problem for a suitable spectral profile of a mode that gives the best possible amount of squeezing (see Appendix B).

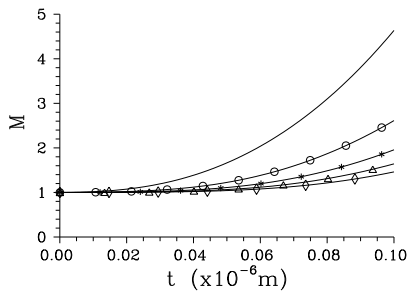


FIG. 12: Enhancement factor \mathcal{M} as a function of the depth t_l of linear corrugation is plotted for the first five transmission peaks: $m = 1$ (solid curve), 2 (solid curve with \circ), 3 (solid curve with $*$), 4 (solid curve with \triangle), and 5 (solid curve with \diamond); $t = 5 \times 10^{-7}$ m.

VIII. SQUEEZED-LIGHT GENERATION - NUMERICAL ANALYSIS FOR PULSED PUMPING

Benefit of a linear corrugation present in the pump field in squeezed-light generation can be roughly judged using the enhancement factor \mathcal{M} defined in Eq. (80). Values of the enhancement factor \mathcal{M} around 4 can be reached in the studied waveguide for the first transmission peak, as documented in Fig. 12.

A detailed analysis of squeezed-light generation in pulsed regime is given for fixed values of the depths of waveguide ($t = 5 \times 10^{-7}$ m) and linear corrugation ($t_l = 5 \times 10^{-8}$ m). The value of enhancement factor \mathcal{M} equals cca 1.5 for the first transmission peak (see Fig. 12). A suitable value of the pump-field linear phase mismatch δ_p^0 is given along the formula in Eq. (41) knowing the value of pump-field linear coupling constant K_p^0 . It depends on the number m counting transmission peaks. The condition in Eq. (35) then provides an optimum value for the nonlinear phase mismatch $\delta_{nl,q}^0$:

$$\delta_{nl,q}^0 = \frac{\delta_p^0}{2} \pm \sqrt{\frac{(\delta_p^0)^2}{4} - |K_p^0|^2}. \quad (97)$$

In Eqs. (41) and (97) there exist four possible combinations of signs. As for squeezing, condition with both signs + gives the same result as that with both signs -. Similarly, conditions with one sign + and one sign - lead to the same amount of squeezing. In our case, the conditions with one sign + and the other sign - give better values of the principal squeeze variance λ_{sF} and that is why we consider them in the following discussion.

Gaussian spectrum $A_{pF}(0, \omega_p)$ of the incident pump pulse is assumed. Its Fourier transform takes the form:

$$A_{pF}(0, \tau) = \sqrt{\frac{\sqrt{2}}{\sqrt{\pi}\tau_p}} \exp \left[-(1 + ia_p) \frac{\tau^2}{\tau_p^2} \right], \quad (98)$$

where τ_p means pump-pulse duration and a_p stands for chirp parameter.

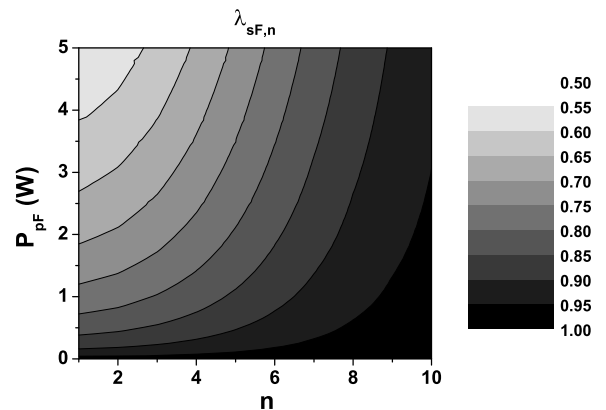


FIG. 13: Contour plot of the principal squeeze variance $\lambda_{sF,n}$ as a function of incident pump power P_{pF} and mode number n ; $\tau_p = 1 \times 10^{-13}$ s, values of the other parameters are the same as in Fig. 12.

In order to observe squeezing in pulsed regime the right choice of eigenmodes is crucial. It occurs that there typically exist several or maximally several tens of eigenmodes that can be considerably squeezed. Values of the principal squeeze variances $\lambda_{sF,n}$ of these modes decrease with the increasing incident pump-field power P_{pF} , as shown in Fig. 13 for 100-fs pump pulse. Measurement of squeezing in the lowest modes can be reached using a suitable profile of a local oscillator in homodyne detection. Eigenmode functions ϕ_n of the first four modes are depicted in Fig. 14. Amplitudes of the functions ϕ_n with even numbers n have maximum at the central frequency ω_s^0 whereas those with odd numbers n are zero. The larger the mode number n the faster the oscillations along the frequency axis ω_s . The eigenmode functions ϕ_n plotted in Fig. 14 are not damped as a consequence of neglecting inter-mode dispersion. As the analytical results given in Eqs. (73) and (76) suggest the inclusion of inter-mode dispersion leads to damped eigenmode functions ϕ_n with a typical time constant τ_s written in Eq. (74). We note that the Bloch-Messiah reduction given in Eq. (93) can be done such that the left and right eigenvectors (contained in matrices \mathbf{X} and \mathbf{Y}) coincide.

Shortening of the pump pulse keeping its energy fixed results in lower values of the principal squeeze variances $\lambda_{sF,n}$ (see Fig. 15). This reflects the fact that shortening of the pump pulse leads to concentration of its energy into a smaller area inside the nonlinear medium and this increases efficiency of the nonlinear process. Lower values of the principal squeeze variances $\lambda_{sF,n}$ then naturally occur. Alternatively we may argue that the shorter the pump-pulse duration τ_p the broader the pump-pulse spectrum $A_{pF}(0, \omega_p)$ and also the better the ability to excite the lowest eigenvectors ϕ_n having the lowest values of $\lambda_{sF,n}$. In cw limit ($\tau_p \rightarrow \infty$), the value of $\lambda_{sF,0}$ belonging to the lowest eigenmode equals cca 0.9 when

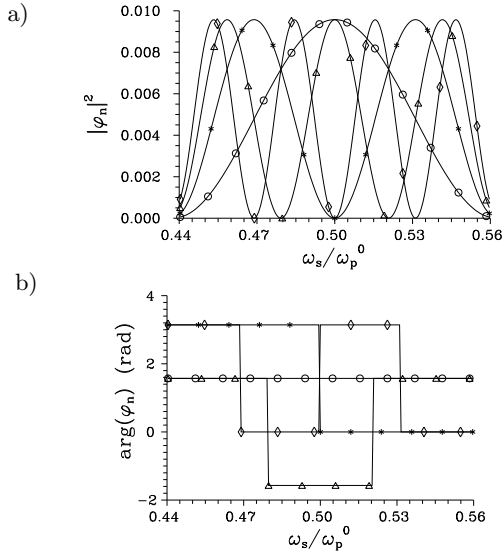


FIG. 14: Amplitude squared $|\phi_n|^2$ (a) and phase $\arg(\phi_n)$ (b) of the first four eigenmode functions ϕ_n as they depend on the normalized frequency ω_s/ω_p^0 ; $n=1$ (solid curve with \circ), 2 (solid curve with $*$), 3 (solid curve with \triangle), and 4 (solid curve with \diamond); $\tau_p = 1 \times 10^{-13}$ s, $P_{pF} = 2$ W, values of the other parameters are the same as in Fig. 12.

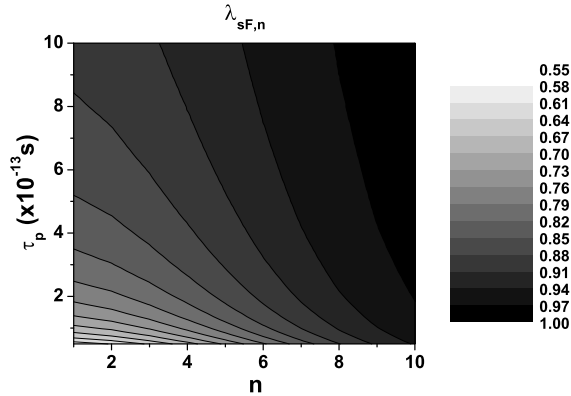


FIG. 15: Contour plot of the principal squeeze variance $\lambda_{sF,n}$ as it depends on the pump-pulse duration τ_p and mode number n ; $P_{pF} = 2$ W, values of the other parameters are the same as in Fig. 12.

pumped by the power of 2 W. On the other hand, cw model discussed in Sec. IV gives the value of λ_{sF} cca 0.3, i.e. cw model predicts higher squeezing of the second-subharmonic field. The main difference between cw and pulsed models is that energy converted from the pump field goes into many modes of the second-subharmonic field in the pulsed model whereas there is only one (effective) mode in the second-subharmonic field in cw model. Thus many modes in the pulsed model compete and as a consequence they cannot reach such low values of the

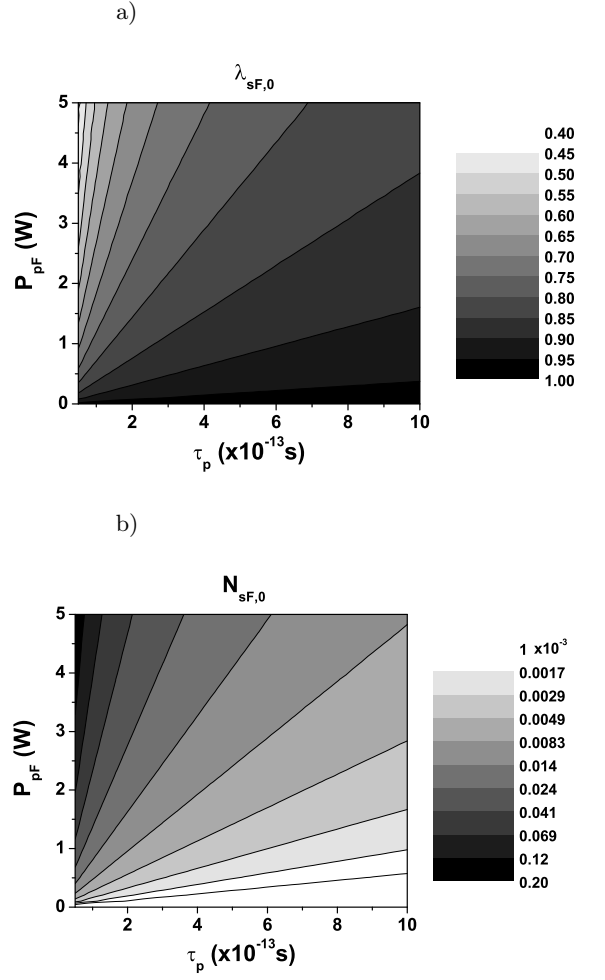


FIG. 16: Contour plots of the principal squeeze variance $\lambda_{sF,0}$ (a) and number $N_{sF,0}$ of photons leaving the waveguide (b) as they depend on incident pump power P_{pF} and pump-pulse duration τ_p for $n = 0$. Logarithmic scale is used on the z axis in (b). Values of parameters are the same as in Fig. 12.

principal squeeze variance λ_{sF} as those provided by cw model.

Only the lowest eigenmode can be measured in optimum homodyne detection in which a local oscillator has shape of the eigenmode function ϕ_0 . Attainable values of the principal squeeze variance $\lambda_{sF,0}$ for a broad range of values of pump-pulse duration τ_p and incident pump-pulse power P_{pF} are shown in Fig. 16a. The number $N_{sF,0}$ of photons leaving the waveguide depicted in Fig. 16b clearly shows, after comparison with the graph in Fig. 16a, that the better the conversion of energy into the lowest eigenmode the better the squeezing in this mode. For example, an incident pump pulse having 100 fs and power of 2 W generates a second-subharmonic field with the lowest eigenmode reaching the value $\lambda_{sF,0} = 0.65$.

The obtained results show that the waveguide made of LiNbO₃ can produce pulsed squeezed light being emitted in the process of second-subharmonic generation. A linear periodic corrugation with appropriate parameters and sensitive to a pump field enhances considerably the nonlinear process.

The analyzed waveguide can serve also as a source of light with sub-Poissonian photon-number statistics. Origin of these nonclassical states having suppressed fluctuations in their photon numbers lies in nonlinear interaction, similarly as in the case of squeezed-light generation. Suitable conditions for generation of light with sub-Poissonian photon-number statistics are similar to those needed for observation of squeezed light and analyzed in detail in the report. This similarity has been elucidated in detail in [45, 46] for three-mode interaction. It allows to use directly the results obtained for squeezed light also in the analysis of suitable conditions for the generation of light with sub-Poissonian photon-number statistics.

IX. CONCLUSIONS

We have shown that an additional scattering of two nonlinearly interacting optical fields caused by a small linear periodic corrugation at the surface of a waveguide can lead to an enhancement of the nonlinear process thus resulting in higher generation rates and better values of squeezing. To observe this effect the natural nonlinear phase mismatch has to be nonzero in order to match with periodic oscillations caused by scattering at the corrugation. Under these conditions, better values of squeezing as well as higher values of intensities of both interacting fields (pump and second-subharmonic) can be reached in comparison with a perfectly quasi-phase-matched waveguide. A linear corrugation can be designed to match either the pump or the second-subharmonic field, or even both of them. Origin of the enhancement of nonlinear interaction lies in constructive interference of scattered light leading to spatial localization. Optimum conditions for this enhancement have been found approximately using analytical approach and confirmed numerically. In practise, the best results are reached with the deepest possible corrugation. Periods of linear corrugation and periodical poling are then determined from the model. In pulsed regime a suitable choice of eigenmodes in the second-subharmonic field is crucial to reach high levels of squeezing. The shorter the pump pulse the better the values of squeezing.

The obtained results have shown that nonlinear planar waveguides with periodically corrugated surfaces represent a promising source of squeezed light for integrated optoelectronics under the conditions excluding nonlinear medium embedded inside a cavity.

APPENDIX A: MODES OF AN ANISOTROPIC WAVEGUIDE

Mode of the considered waveguide [53] depicted in Fig. 1 is given as a solution of the wave equation written in Eq. (7). The waveguide is made of LiNbO₃ crystal using the method of proton exchange. The crystallographic z axis coincides with the x axis of the coordinate system (see Fig. 1). Ordinary ($n_{s,o}$) and extraordinary ($n_{s,e}$) indices of refraction of LiNbO₃ valid for the substrate and used in calculations are given as:

$$\begin{aligned} n_{s,a}^2 &= A_a + \frac{B_a}{\lambda^2 - C_a} - D_a \lambda^2, \quad a = o, e, \\ A_o &= 4.91300, B_o = 0.118717, \\ C_o &= 0.045932, D_o = 0.0278, \\ A_e &= 4.57906, B_e = 0.099318, \\ C_e &= 0.042286, D_e = 0.0224; \end{aligned} \quad (\text{A1})$$

wavelength λ is in μm . After proton exchange, ordinary ($n_{w,o}$) and extraordinary ($n_{w,e}$) indices of refraction of LiNbO₃ characterizing the waveguide are reached:

$$\begin{aligned} n_{w,o} &= n_{s,o} - \frac{1}{3} \delta n, \\ n_{w,e} &= n_{s,e} + \delta n, \\ (\delta n)^2 &= A_1 + \frac{B_1}{\lambda^2 - C_1} - D_1 \lambda^2; \\ A_1 &= 0.007596, B_1 = 0.001129, \\ C_1 &= 0.116926, D_1 = -0.0003126. \end{aligned} \quad (\text{A2})$$

We assume that air is present above the waveguide, i.e.:

$$n_u = 1. \quad (\text{A3})$$

Because only the extraordinary index of refraction of LiNbO₃ increases during proton exchange, only TM waves can be guided. For this reason, instead of solving Eq. (7) for x and z components of the electric-field mode functions \mathbf{e}_a , we solve the following equation for the only nonzero y component of the magnetic-field mode functions $\mathbf{h}_a(x)$ (fields are assumed to be homogeneous along the y axis) [41]:

$$\frac{d^2 \mathbf{h}_a(x)}{dx^2} + \left[-\frac{\bar{\epsilon}_{zz}(x, \omega_a)}{\bar{\epsilon}_{xx}(x, \omega_a)} \beta_a^2 + \frac{\bar{\epsilon}_{zz}(x, \omega_a) \omega_a^2}{c^2} \right] \mathbf{h}_a(x) = 0. \quad (\text{A4})$$

Solution of Eq. (A4) for the y component of magnetic-field mode function $\mathbf{h}_a(x)$ ($a = p, s$) can be written as:

$$\begin{aligned} [\mathbf{h}_a(x)]_y &= -C_a \frac{h_a}{\tilde{q}_a} \exp(-qx), \quad x > 0; \\ &= C_a \left[-\frac{h_a}{\tilde{q}_a} \cos(h_a x) + \sin(h_a x) \right], \quad 0 < x < -t; \\ &= -C_a \left[\frac{h_a}{\tilde{q}_a} \cos(h_a t) + \sin(h_a t) \right] \exp(p_a t) \\ &\quad \times \exp(p_a x), \quad x < -t; \end{aligned} \quad (\text{A5})$$

where C_a denotes a normalization constant. We have the following expressions for coefficients h_a , q_a , p_a , \tilde{p}_a , and \tilde{q}_a for the considered orientation of LiNbO₃:

$$\begin{aligned} h_a &= \sqrt{\left(\frac{n_{w,o}(\omega_a)\omega_a}{c}\right)^2 - \left(\frac{n_{w,o}(\omega_a)}{n_{w,e}(\omega_a)}\beta_a\right)^2}, \\ q_a &= \sqrt{\beta_a^2 - \left(\frac{n_u\omega_a}{c}\right)^2}, \\ p_a &= \sqrt{\left(\frac{n_{s,o}(\omega_a)}{n_{s,e}(\omega_a)}\beta_a\right)^2 - \left(\frac{n_{s,o}(\omega_a)\omega_a}{c}\right)^2}, \\ \tilde{p}_a &= \frac{n_{w,o}^2(\omega_a)}{n_{s,o}^2(\omega_a)}p_a, \\ \tilde{q}_a &= \frac{n_{w,o}^2(\omega_a)}{n_u^2}q_a. \end{aligned} \quad (\text{A6})$$

Solution written in Eq. (A5) holds provided that the following dispersion relation giving the propagation constant β_a as a function of the frequency ω_a is valid:

$$\tan(h_a t) = \frac{h_a(\tilde{p}_a + \tilde{q}_a)}{h_a^2 - \tilde{p}_a \tilde{q}_a}. \quad (\text{A7})$$

We note that possible solutions of Eq. (A7) for the propagation constant β_a lie in the interval $n_{s,e}(\omega_a)\omega_a/c \leq \beta_a \leq n_{w,e}(\omega_a)\omega_a/c$.

Components of the electric-field mode function $\mathbf{e}_a(x)$ can be derived from the magnetic-field mode functions $\mathbf{h}_a(x)$ along the relations:

$$\begin{aligned} [\mathbf{e}_a(x)]_x &= \frac{\beta_a}{\omega_a \epsilon_0 \bar{\epsilon}_{xx}(x, \omega_a)} [\mathbf{h}_a(x)]_y, \\ [\mathbf{e}_a(x)]_y &= 0, \\ [\mathbf{e}_a(x)]_z &= -\frac{i}{\omega_a \epsilon_0 \bar{\epsilon}_{zz}(x, \omega_a)} \frac{d[\mathbf{h}_a(x)]_y}{dx}. \end{aligned} \quad (\text{A8})$$

The normalization constants C_a occurring in Eqs. (A5) are determined from the condition that the mode functions $\mathbf{e}_a(x)$ describe one photon with energy $\hbar\omega_a$ inside the waveguide (of length L and thickness Δy):

$$\begin{aligned} 2\epsilon_0 \Delta y L \int_{-\infty}^{\infty} dx \left[\bar{\epsilon}_{xx}(x, \omega_a) |[\mathbf{e}_a(x)]_x|^2 \right. \\ \left. + \bar{\epsilon}_{zz}(x, \omega_a) |[\mathbf{e}_a(x)]_z|^2 \right] = \hbar\omega_a. \end{aligned} \quad (\text{A9})$$

Corrugation on the surface causes periodic changes of values of permittivity ϵ for $x \in (0, -t_l)$ (see Fig. 1) and we have $\epsilon_{\pm 1} = i(\bar{\epsilon} - 1)/(\pi\bar{\epsilon})$ in this case using Eqs. (2) and (3). If the waveguide is periodically poled $\mathbf{d}_{\pm 1} = -2i/\pi\mathbf{d}$ in Eq. (5) and the remaining coefficients may be omitted. Using the electric-field mode functions \mathbf{e}_a determined in Eqs. (A8), linear (K_s , K_p) and nonlinear ($K_{nl,0}$, $K_{nl,\pm 1}$) coupling constants defined in Eqs. (11) and (12) can be rearranged into the form:

$$K_a = \frac{i\omega_a^2}{2\pi c^2 \beta_a} \left[\frac{n_{w,e}^2(\omega_a) - 1}{n_{w,e}^2(\omega_a)} \int_{-t_l}^0 dx |[\mathbf{e}_a(x)]_x|^2 \right.$$

$$\begin{aligned} &+ \frac{n_{w,o}^2(\omega_a) - 1}{n_{w,o}^2(\omega_a)} \int_{-t_l}^0 dx |[\mathbf{e}_a(x)]_z|^2 \Big] \\ &\times \left[\int_{-\infty}^{\infty} dx (|[\mathbf{e}_a(x)]_x|^2 + |[\mathbf{e}_a(x)]_z|^2) \right]^{-1}, \\ &a = p, s, \end{aligned} \quad (\text{A10})$$

$$\begin{aligned} K_{nl,0} &= \frac{i\omega_s^2}{2c^2 \beta_s} \int_{-\infty}^0 dx \mathbf{d} \cdot \mathbf{e}_p(x) \mathbf{e}_s^*(x) \mathbf{e}_s^*(x) \\ &\times \left[\int_{-\infty}^{\infty} dx (|[\mathbf{e}_s(x)]_x|^2 + |[\mathbf{e}_s(x)]_z|^2) \right]^{-1}, \end{aligned} \quad (\text{A11})$$

$$K_{nl,\pm 1} = -\frac{2i}{\pi} K_{nl,0}. \quad (\text{A12})$$

Nonzero coefficients of the nonlinear tensor \mathbf{d} of LiNbO₃ used in calculations are the following:

$$\begin{aligned} d_{zzz} &= -d_{zyy} = -d_{yyz} = 3.1 \times 10^{-12} \text{mV}^{-1}, \\ d_{xyy} &= d_{xzz} = d_{zzx} = d_{yyx} = 5.87 \times 10^{-12} \text{mV}^{-1}, \\ d_{xxx} &= 41.05 \times 10^{-12} \text{mV}^{-1}. \end{aligned} \quad (\text{A13})$$

APPENDIX B: AN OPTIMUM MODE FOR PULSED SQUEEZED LIGHT

We look for a suitable linear combination of output operator amplitudes $\hat{a}_{s_F,i}^{\text{out}}$ that minimizes the value of principal squeeze variance λ_{s_F} [54]:

$$\hat{a}_{s_F}^{\text{out}} = \sum_i t_i \hat{a}_{s_F,i}^{\text{out}}. \quad (\text{B1})$$

Coefficients t_i fulfill the normalization condition $\sum_i |t_i|^2 = 1$. Using Eqs. (24) and (26) the principal squeeze variance λ_{s_F} as a function of t_i and t_i^* can be expressed in the following form:

$$\lambda_{s_F}(\mathbf{t}, \mathbf{t}^*) = 1 + 2\mathbf{t}^\dagger \mathbf{W}_1 \mathbf{t} - 2|\mathbf{t} \mathbf{W}_2 \mathbf{t}|. \quad (\text{B2})$$

Vector \mathbf{t} occurring in Eq. (B2) is composed of coefficients t_i . Matrices \mathbf{W}_1 and \mathbf{W}_2 are defined as:

$$\begin{aligned} \mathbf{W}_1 &= \mathbf{V}^* \mathbf{V}^T, \\ \mathbf{W}_2 &= \mathbf{U} \mathbf{V}^T, \end{aligned} \quad (\text{B3})$$

where the matrices \mathbf{U} and \mathbf{V} are given in Eq. (91).

Instead of using coefficients t_i , we define new coefficients s_i along the relation:

$$\mathbf{s} = \mathbf{t} \exp(-i\varphi/2), \quad \exp(i\varphi) = \frac{\mathbf{t}^T \mathbf{W} \mathbf{t}}{|\mathbf{t}^T \mathbf{W} \mathbf{t}|}. \quad (\text{B4})$$

Minimum value of the principal squeeze variance λ_{s_F} is reached for the values of coefficients s_i and s_i^* that minimize the function f :

$$f(\mathbf{s}, \mathbf{s}^*) = 1 + 2\mathbf{s}^\dagger \mathbf{W}_1 \mathbf{s} - 2\mathbf{s} \mathbf{W}_2 \mathbf{s} - \mu \mathbf{s}^\dagger \cdot \mathbf{s}, \quad (\text{B5})$$

μ denotes a Lagrange multiplier for the condition $\mathbf{s}^\dagger \cdot \mathbf{s} = 1$.

Derivation of the function f given in Eq. (B5) with respect to coefficients s_i^* results in the condition:

$$2\mathbf{W}_1\mathbf{s} = \mu\mathbf{s}. \quad (\text{B6})$$

This condition can be rearranged using Eqs. (B3):

$$\mathbf{V}\mathbf{V}^\dagger\mathbf{s}^* = \frac{\mu}{2}\mathbf{s}^*. \quad (\text{B7})$$

On the other hand, the Bloch-Messiah reduction of matrix \mathbf{V} in Eq. (93) provides the formula

$$\mathbf{V}\mathbf{V}^\dagger\mathbf{X}_i = (\Lambda_{\mathbf{V}})_{ii}^2\mathbf{X}_i \quad (\text{B8})$$

valid for i th eigenvalue $(\Lambda_{\mathbf{V}})_{ii}$ and eigenvector \mathbf{X}_i . Comparison of Eqs. (B7) and (B8) leads to the conclusion that the complex conjugated vector \mathbf{s}^* coincides with the i th eigenvector \mathbf{X}_i and the Lagrange multiplier μ fulfills the relation $\mu = 2(\Lambda_{\mathbf{V}})_{ii}^2$.

Because we look for a minimum value of the principal squeeze variance λ_{s_F} the appropriate mode is characterized by the largest eigenvalue $(\Lambda_{\mathbf{V}})_{ii}$ [compare Eq. (95)].

This mode has also to fulfill the condition obtained by derivating the function f written in Eq. (B5) with respect to coefficients s_i :

$$2\mathbf{s}^\dagger\mathbf{W}_1 - 2\mathbf{s}^T\mathbf{W}_2 - 2\mathbf{W}_2\mathbf{s} - \mu\mathbf{s}^\dagger = 0. \quad (\text{B9})$$

The use of expresions in Eqs. (B3) and (B6) transforms Eq. (B9) into the final form:

$$\mathbf{V}\mathbf{U}^T\mathbf{s} + \mathbf{s}^T\mathbf{U}\mathbf{V}^T = 0. \quad (\text{B10})$$

ACKNOWLEDGMENTS

The authors thank A. Lukš and V. Peřinová for discussions and help with analytical computations. This material is based upon the work supported by the European Research Office of the US Army under the Contract No. N62558-05-P-0421. Also support coming from cooperation agreement between Palacký University and University La Sapienza in Rome is acknowledged.

-
- [1] J.A. Armstrong, N. Bloemberger, J. Ducuing, and P.S. Pershan, *Phys. Rev.* **127**, 1918 (1962).
 - [2] J. Peřina, *Quantum Statistics of Linear and Nonlinear Optical Phenomena* (Kluwer, Dordrecht, 1991).
 - [3] L. Mandel and E. Wolf, *Optical Coherence and Quantum Optics* (Cambridge Univ. Press, Cambridge, 1995).
 - [4] V.V. Dodonov, *J. Opt. B: Quantum Semiclass. Opt.* **4**, R1 (2002).
 - [5] W. Vogel and D.-G. Welsch, *Quantum Optics* (Akademie Verlag, Berlin, 1994).
 - [6] H.-A. Bachor and T.C. Ralph, *A Guide to Experiments in Quantum Optics* (Wiley-VCH, Weinheim, 2004).
 - [7] W. Schleich and A. Wheeler, *J. Opt. Soc. Am. B* **4**, 1715 (1987).
 - [8] J. Peřina and J. Bajer, *Phys. Rev. A* **41**, 516 (1990).
 - [9] E. Waks, E. Diamanti, B.C. Sanders, S.D. Bartlett, and Y. Yamamoto, *Phys. Rev. Lett.* **92**, 113602 (20024).
 - [10] Z.Y. Ou, *Phys. Rev. A* **49**, 2106 (1994).
 - [11] R.-D. Li and P. Kumar, *Optics Lett.* **18**, 1961 (1993).
 - [12] R.-D. Li and P. Kumar, *Phys. Rev. A* **49**, 2157 (1994).
 - [13] D.K. Serkland, M.M. Fejer, R.L. Byer, and Y. Yamamoto, *Optics Lett.* **20**, 1649 (1995).
 - [14] D.K. Serkland, P. Kumar, M.A. Arbore, and M.M. Fejer, *Optics Lett.* **22**, 1497 (1997).
 - [15] X. Yu, L. Scaccabarozzi, J.S. Harris, Jr., P.S. Kuo, and M.M. Fejer, *Optics Express* **13**, 10742 (2005).
 - [16] J. Huang, X.P. Xie, C. Langrock, R.V. Roussev, D.S. Hum, and M.M. Fejer, *Optics Lett.* **31**, 604 (2006).
 - [17] A.W. Schober, M. Charbonneau-Lefort, and M.M. Fejer, *J. Opt. Soc. Am. B* **22**, 1699 (2005).
 - [18] M.J. Lawrence, R.L. Byer, M.M. Fejer, W. Bowen, P.K. Lam, and H.-A. Bachor, *J. Opt. Soc. Am. B* **19**, 1592 (2002).
 - [19] P. Dong and A.G. Kirk, *Phys. Rev. Lett.* **93**, 133901 (2004).
 - [20] J. Peřina Jr. and J. Peřina, *Progress in Optics* **41**, Ed. E. Wolf, (Elsevier Science, Amsterdam, 2000), p. 362.
 - [21] J.D. Joannopoulos, R.D. Meade, and J.N. Winn, *Photonic Crystals: Molding the Flow of Light* (Princeton University Press, Princeton, 1995).
 - [22] M. Bertolotti, C.M. Bowden, and C. Sibilía, *Nanoscale Linear and Nonlinear Optics*, AIP Vol. 560 (AIP, Melville, 2001).
 - [23] J.W. Haus, R. Viswanathan, M. Scalora, A.G. Kalocsai, J.D. Cole, and J. Theimer, *Phys. Rev. A* **57**, 2120 (1998).
 - [24] D. Pezzetta, C. Sibilía, M. Bertolotti, J.W. Haus, M. Scalora, M.J. Bloemer, and C.M. Bowden, *J. Opt. Soc. Am. B* **18**, 1326 (2001).
 - [25] D. Tricca, C. Sibilía, S. Severini, M. Bertolotti, M. Scalora, C.M. Bowden, and K. Sakoda, *J. Opt. Soc. Am. B* **21**, 671 (2004).
 - [26] D. Pezzetta, C. Sibilía, M. Bertolotti, R. Ramponi, R. Osellame, M. Marangoni, J.W. Haus, M. Scalora, M.J. Bloemer, and C.M. Bowden, *J. Opt. Soc. Am. B* **19**, 2102 (2002).
 - [27] K. Sakoda, *J. Opt. Soc. Am. B* **19**, 2060 (2002).
 - [28] M.J. Werner, M.G. Raymer, M. Beck, and P.D. Drummond, *Phys. Rev. A* **52**, 4202 (1995).
 - [29] P. Scotto, *Phys. Rev. A* **68**, 033814 (2003).
 - [30] M. Bache, P. Scotto, R. Zambrini, M. San Miguel, and M. Saffman, *Phys. Rev. A* **66**, 013809 (2002).
 - [31] P. Kumar, O. Aytur, and J. Huang, *Phys. Rev. Lett.* **64**, 1015 (1990).
 - [32] R.S. Bennink and R.W. Boyd, *Phys. Rev. A* **66**, 053815 (2002).
 - [33] S.L. Braunstein, *Phys. Rev. A* **71**, 055801 (2005).

- [34] W. Wasilewski, A.I. Lvovsky, K. Banaszek, and C. Radzewicz, Phys. Rev. A **73**, 063819 (2006); arXiv:quant-ph/0512215.
- [35] A.I. Lvovsky, W. Wasilewski, and K. Banaszek, J. Mod. Opt. **54**, 721 (2007); arXiv:quant-ph/0601170.
- [36] M. Sasaki and S. Suzuki, arXiv:quant-ph/0512073.
- [37] M. Scalora, M.J. Bloemer, A.S. Manka, J.P. Dowling, C.M. Bowden, R. Viswanathan, and J.W. Haus, Phys. Rev. A **56**, 3166 (1997).
- [38] G. D'Aguanno, M. Centini, M. Scalora, C. Sibilial, Y. Dumeige, P. Vidakovic, J.A. Levenson, M.J. Bloemer, C.M. Bowden, J.W. Haus, and M. Bertolotti, Phys. Rev. E **64**, 016609 (2001).
- [39] Y. Dumeige, P. Vidakovic, S. Sauvage, I. Sagnes, J.A. Levenson, C. Sibilial, M. Centini, G. D'Aguanno, and M. Scalora, Appl. Phys. Lett. **78**, 3021 (2001).
- [40] J. Peřina Jr., O. Haderka, C. Sibilial, M. Bertolotti, and M. Scalora, Squeezed-light generation in a photonic band-gap nonlinear planar waveguide, sent for publication.
- [41] A.W. Snyder and J.D. Love, *Optical Waveguide Theory*, (Chapman & Hall, London, 1983).
- [42] J. Peřina and J. Peřina Jr., J. Mod. Opt. **43**, 1956 (1996).
- [43] N. Korolkova and J. Peřina, Opt. Commun. **137**, 263 (1997).
- [44] M. Fiurášek and J. Peřina, Phys. Rev. A **62**, 033808 (2000).
- [45] J. Peřina Jr., C. Sibilial, D. Tricca, and M. Bertolotti, Phys. Rev. A **70**, 043816 (2004); arXiv:quant-ph/0405051.
- [46] J. Peřina Jr., C. Sibilial, D. Tricca, and M. Bertolotti, Phys. Rev. A **71**, 043813 (2005); arXiv:quant-ph/0412208.
- [47] W.H. Press, S.A. Teukolsky, W.T. Vetterling, and B.P. Flannery, *Numerical Recipes* (Cambridge University Press, Cambridge, 1996).
- [48] A.W. Schober, M.M. Fejer, S. Carrasco, and L. Torner, Optics Lett. **30**, 1983 (2005).
- [49] A. Luis, J. Peřina, Quantum Semiclass. Optics **8**, 39 (1996).
- [50] T.E. Keller and M.H. Rubin, Phys. Rev. A **56**, 1534 (1997).
- [51] J. Peřina Jr., A.V. Sergienko, B.M. Jost, B.E.A. Saleh, and M.C. Teich, Phys. Rev. A **59**, 2359 (1999).
- [52] G. Di Giuseppe, L. Haiberger, F. De Martini, and A.V. Sergienko, Phys. Rev. A **56**, R21 (1997).
- [53] P. Yeh, *Optical Waves in Layered Media* (Wiley, New York, 1988).
- [54] A. Lukš, private communication.